

1 **The potential of Tidal River Management for flood alleviation in South Western** 2 **Bangladesh**

3 Mohammed Sarfaraz Gani Adnan ^{a,c*}, Rocky Talchabhadel ^b, Hajime Nakagawa ^b, Jim W.
4 Hall ^a

5

6 ^a Environmental Change Institute, School of Geography and the Environment, University of Oxford,
7 South Parks Road, OX13QY Oxford, United Kingdom

8 ^b Disaster Prevention Research Institute, Kyoto University, Japan

9 ^c Department of Urban and Regional Planning, Chittagong University of Engineering and Technology
10 (CUET), Chittagong 4349, Bangladesh

11

12 **Abstract**

13 Reduced sediment deposition, land subsidence, channel siltation, and salinity intrusion has been an
14 unintended consequence of the construction of polders in the south western delta of Bangladesh in the
15 1960s. Tidal River Management (TRM) is a process that is intended to temporarily reverse these
16 processes and restore sediment deposition and land elevation at the low-lying sites, known as ‘beels’,
17 where TRM is carried out. However, there is limited evidence to prioritise sites for TRM on the basis
18 of its potential effectiveness at alleviating flooding. In this study, the south western delta of Bangladesh
19 was classified according to different flood susceptible zones. In south western Bangladesh, the major
20 portion of agricultural and aquaculture land is located within flood susceptible zones (65% and 81%,
21 respectively). 44.5% of the total population in embanked regions live in areas classified as being flood
22 susceptible. This study identified 106 ‘beels’ suitable for TRM. Modelling of potential sediment
23 deposition predicted that the consequent increase in land elevation could be up to 1.4m in five years,
24 which would alleviate land subsidence and modify several geomorphological factors such as aspect,
25 slope, curvature, and Stream Power Index (SPI). Implementation of TRM at these sites could potentially
26 reduce the probability of annual flooding from 0.86 (on average) to 0.57 (on average). Therefore, TRM
27 could lower the flood susceptible area by 35% in suitable ‘beels’. Whilst during the implementation of
28 TRM agriculture has to cease for a few years, a systematic programme of TRM could result in a long-
29 term increase in agricultural production by reducing flood susceptibility of agricultural lands in delta
30 regions.

31 Key words: Tidal River Management; flood susceptibility; frequency ratio; logistic regression;
32 sediment transportation; Bangladesh coastal region

33

34

35 1. Introduction

36 Pluvial flooding during the monsoon period affects the south western coastal region of Bangladesh
37 annually (Warner et al., 2018), inundating agricultural lands and damaging people's livelihoods (Alam
38 et al., 2017; Awal, 2014). This form of flood occurs either due to a short term intense or prolonged low
39 to moderate level precipitation (Falconer et al., 2009). Pluvial flooding has become much more severe
40 in this region because of land subsidence, siltation in riverbeds restricting drainage, and land use change
41 e.g., the encroachment of drainage channels (Alam et al., 2017).

42 Following a major cyclone and storm surge flood in 1953, the East Pakistan Water and Power
43 Development Authority (now the Bangladesh Water Development Board (BWDB)) invested in a major
44 Coastal Embankment Project (CEP). Since 1960, a total of 139 polders (enclosed coastal embankments)
45 were constructed throughout the coastal region, with the stated objective of preventing inundation by
46 saline water of agricultural lands during surge tides and cyclones, increasing agricultural production
47 and ensuring food security (Islam et al., 2016; Warner et al., 2018). The construction of polders resulted
48 in increased agricultural production until the 1980s (Nowreen et al., 2014). On the other hand, the polder
49 system disconnected the delta floodplain from the river channel network, which had the consequences
50 of promoting land subsidence in the embanked areas (Alam et al., 2017; Auerbach et al., 2015; Van
51 Staveren et al., 2017). The embanked region in the south western coast of Bangladesh has lost 1.0-1.5m
52 of land elevation since the construction of the polders (Auerbach et al., 2015). The polder system
53 restricted silts from rivers being deposited onto 'beels' (a local term referring to surface depression),
54 whilst accelerating sedimentation in riverbeds and increasing river water levels. In turn, this prevents
55 gravity drainage systems within the embanked region from functioning properly (Mutahara et al., 2018).
56 As a result, runoff generated from monsoon precipitation accumulates in and floods, polders (Auerbach
57 et al., 2015; Choudhury et al., 2004; Talchabhadel et al., 2018). Projected sea level rise (IPCC, 1996)
58 will increase the tidal water level within the adjacent Bay of Bengal, worsening drainage congestion
59 and pluvial flooding in polders (Awal, 2014). Pluvial floods lead to economic losses either by damaging
60 crops or delaying cultivation of winter crops (*Boro* rice), affecting the livelihood of millions of people
61 across the Ganges-Brahmaputra-Meghna (GBM) delta, and particularly poor and marginal farmers
62 living inside polders (Alam et al., 2017). For instance, a pluvial flood in 2011 inundated more than
63 128,000ha of croplands for 90 days in three south western coastal districts of Bangladesh: Khulna,
64 Satkhira, and Jessore (Awal, 2014).

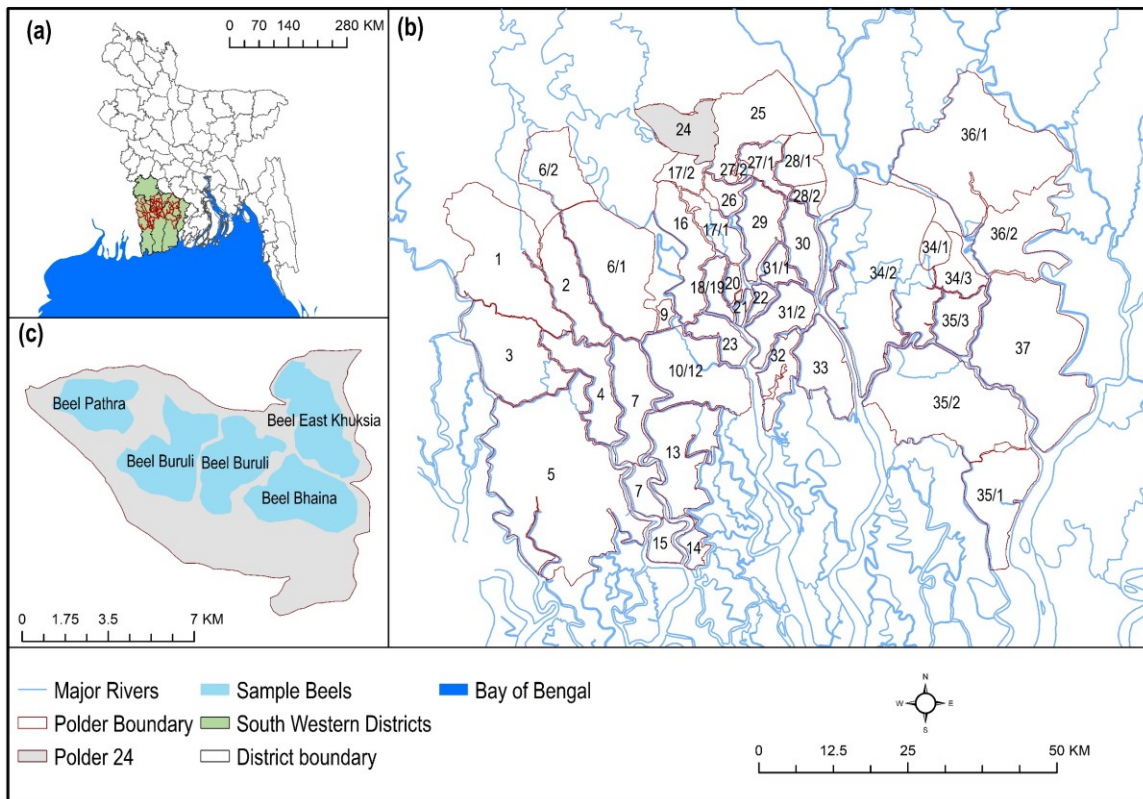
65 Tidal River Management (TRM) has been adopted in an attempt to address the worsening impacts of
66 pluvial flooding, salinity, and siltation in riverbeds, by restoring sedimentation in low-lying 'beels'. The
67 idea of TRM is to bring sediment-carrying tidal water into selected 'beels' two times a day through a
68 controlled breaching in polders, to allow sedimentation and elevate the land (Amir and Khan, 2019;
69 Gain et al., 2017; Masud et al., 2018; Seijger et al., 2019; Talchabhadel et al., 2018). Although

70 historically a community-driven approach, the BWDB has been responsible for implementing TRM
71 since 1997. From 1991 to 2013, TRM has been implemented (either by local people or the BWDB) in
72 12 out of 35 designated 'beels' in the south western coastal zone (Gain et al., 2017; Masud et al., 2018).
73 Implementation of TRM in the south western embanked region is still an ongoing process (Gain et al.,
74 2017). However, governance issues (e.g. disagreement about TRM sites and issues with compensation)
75 were reported during the implementation and operation of TRM projects (Gain et al., 2017; Mutahara
76 et al., 2018). Since TRM makes the 'beel' unsuitable for crop production during the implementation
77 period (Masud et al., 2018), an explicit engagement of different stakeholders (landowners and
78 agricultural workers who are fully or partially dependent on the land in TRM sites) is required from
79 project planning to implementation phases (Mutahara et al., 2018).

80 Existing studies have described both positive and negative impacts of TRM projects on local
81 communities and the environment (Amir and Khan, 2019; Gain et al., 2017; Masud et al., 2018;
82 Mutahara et al., 2018). For instance, the operation of TRM in 'beel' Bhaina (1997-2001) led to a raise
83 in land elevation by 1m on average and consequently increased the depth and width of the adjacent Hari
84 River by 10-12m and 2-3 times, respectively (Gain et al., 2017; Mutahara et al., 2018). On the other
85 hand, an unplanned TRM operation could lead to riverbank erosion, salinity intrusion, and inundation
86 in built-up areas (Gain et al., 2017; Talchabhadel et al., 2018). For instance, in 'beel' Khuksia, an
87 unplanned implementation of TRM, without sufficient cooperation between stakeholders and
88 government agencies, resulted in several disruptions during implementation (2006-2012). Thus,
89 inundation problems remained after the implementation of TRM in Khukshia (Figure 1 (c)) because of
90 an uneven land elevation caused by an uneven distribution of deposited sediments (Gain et al., 2017).
91 Also, various environmental and economic issues can arise during the implementation of TRM (Masud
92 et al., 2018). These issues include an increase in salinity intrusion, inundation of agricultural lands,
93 riverbank erosion, and disruption of transport services (Gain et al., 2017).

94 Evaluating the impact of TRM on flooding is a complex process because (1) the rate of sedimentation
95 vary spatially and temporally (Gain et al., 2017) and (2) flooding is an outcome of various combinations
96 of geomorphological, hydrological, and anthropogenic processes (Khosravi et al., 2016; Pradhan et al.,
97 2010; Tehrany et al., 2014a). Although some benefits of TRM have been reported in the literature (Amir
98 and Khan, 2019; Gain et al., 2017), there remains a lack of evidence of how the implementation of TRM
99 will change the actual mechanism of flooding, leading to a potential change in the extent of the flood
100 susceptible area in embanked regions. Care should be given to identify areas suitable for operating TRM
101 to avoid adverse impacts on society and the environment. To address these challenges, (1) flood
102 mechanisms in the south western embanked region of Bangladesh were analysed, estimating the
103 influence of various flood causative factors on flood susceptibility, and (2) the impact of TRM on flood
104 susceptibility was quantified, modelling sediment transportation and deposition in suitable TRM sites

105 comparing flood susceptibility before and after TRM implementation, in order to prioritise suitable
 106 sites.



107

108

Figure 1: Study area map

109 2. Materials and methods

110 This study was conducted in two stages. First, the influence of various factors on flooding was analysed
 111 to derive a flood susceptibility map. Second, potential TRM sites were identified to model sediment
 112 deposition in those areas. The potential impact of TRM on flooding was investigated by comparing
 113 flood susceptibility ‘before and after’ the implementation of TRM. To estimate flood susceptibility
 114 during the post-TRM scenario, geomorphological changes due to sedimentation in suitable sites were
 115 incorporated in the model.

116 2.1. Study area

117 The study focused on the south western coastal region of Bangladesh, containing 44 polders located in
 118 five coastal districts: Bagerhat, Jessore, Khulna, Pirojpur, and Satkhira (Figure 1 (a)). Approximately
 119 5.3 million people live in this region (WorldPop, 2017), which includes areas from three physiographic
 120 regions of Bangladesh Ganges River floodplains, Ganges tidal floodplain, and old floodplain basins
 121 (Brammer, 2014). This low-lying deltaic region has a mean elevation of 3.5 m and is heavily intersected
 122 by tidal rivers. The Bangladesh Sundarban mangrove forest is located in the south of the study area.

123 Embankments were built in the study area from the 1960s to 1980s to protect about 5187 km² of land
124 (WARPO, 2018). The region is mainly characterized by aquaculture lands and rural settlements
125 (Abdullah et al., 2019). Although the region is prone to three types of flooding — pluvial, fluvio-tidal,
126 and surge flood — pluvial flooding is the most frequent form of flooding (Adnan et al., 2019b). Frequent
127 pluvial flooding (locally also referred to as ‘waterlogging’) in the region has decreased agricultural
128 production and may have contributed to out-migration (Wilson et al., 2017). The region receives
129 maximum precipitation during the monsoon months particularly from June to September, generating
130 excess runoff. Inadequate drainage, due to deteriorating drainage channels and unreliable operation of
131 sluice gates, contributes to frequent inundation in the low-lying ‘beels’(Adnan et al., 2019b;
132 Talchabhadel et al., 2018). The current study hypothesized that a loss in land elevation due to land
133 subsidence contributed to a change in different geomorphological conditions determining the
134 probability that an area will be flooded. Restoring sedimentation through TRM will promote a change
135 in those flood conditioning factors, which will reduce the likelihood of flooding in the embanked region.

136 **2.2. Flood inventory mapping**

137 A flood inventory map of the study area was derived, analysing flood observation data obtained from
138 remote-sensing imagery. Adnan et al. (2019b) identified the extent of annual flood inundation in the
139 south western embanked region from 1988 to 2012 and attributed each flood to pluvial, fluvio-tidal,
140 and storm surge flood events. The raster maps of binary (flood and non-flood) flood inundation maps
141 of those 25 years were collected and overlaid in GIS to estimate the number of times (frequency) that
142 different cells within the study area were inundated. Cells that remained flood-free were also identified
143 (Figure S9 (a), supplementary document). The resultant flood inventory map was used to generate
144 random flood and non-flood points for flood susceptibility modelling (Tehrany et al., 2019a). Applying
145 a stratified random sampling method in GIS, we generated a vector layer of 1000 points where flood
146 and non-flood locations were 586 and 414, respectively. The ratio of flood and non-flood locations was
147 determined based on the proportion of the total area either affected or remained flood free during
148 historical flooding, respectively. About 58.6% of the total area was inundated at least once during the
149 floods from 1988 to 2012. The sample locations were split into two groups; 70% of samples (training
150 data) were used to develop the flood susceptibility model and remaining 30% data (test data) were
151 employed for validating the model (Table S2, supplementary document).

152 **2.3. Deriving flood conditioning factors**

153 The accuracy of hazard susceptibility map depends on the selection of hazard conditioning factors
154 (Sabatakakis et al., 2013). Numerous studies have been conducted on flood hazard susceptibility
155 mapping (Alam et al., 2017; Arabameri et al., 2019; Kabenge et al., 2017; Khosravi et al., 2016;
156 Mojaddadi et al., 2017; Tehrany et al., 2014a; Tehrany et al., 2014b; Tehrany et al., 2017), with various
157 combinations of flood conditioning factors being used. However, the selection of factors should be

158 based on the knowledge of morphological characteristics of the region under study (Tehrany et al.,
159 2019a). Based on the knowledge obtained from the literature, initially 14 flood conditioning factors
160 were selected under five broad categories: topographic, anthropogenic, geological, hydrological, and
161 locational factors. Raster layers of the 14 flood conditioning factors were generated at 30m spatial
162 resolution. Data used to produce those layers are listed in Table S1 of the supplementary document.

163 Topographic factors included aspect, elevation, slope, curvature, and land subsidence (Figure S1,
164 supplementary document). Raster layers of the slope, aspect, and curvature were derived from the
165 Advanced Land Observing Satellite (ALOS) Digital Elevation Model (DEM) (JAXA, 2015) in ArcGIS.
166 Aspect denotes the direction of slope (Zevenbergen and Thorne, 1987), indicating the extent of
167 precipitation and sunshine that an area would receive (Tehrany et al., 2017), which affects the water
168 balance of an area (Singh et al., 2004). Together, elevation and slope influence the occurrence of
169 flooding, as areas with a lower elevation and slope are more susceptible to flooding (Kabenge et al.,
170 2017; Khosravi et al., 2016; Tehrany et al., 2014a; Tehrany et al., 2017). In relation to curvature,
171 surfaces with flat or concave characteristics are more prone to inundation (Tehrany et al., 2017). This
172 study assumes the land subsidence rate as a linear estimate (Brown and Nicholls, 2015). A layer of
173 annual land subsidence rate was collected from Adnan et al. (2019b) where the natural neighbour
174 interpolation method was applied in GIS to convert 205 point measurement of net subsidence (Brown
175 and Nicholls, 2015) into a raster. Since the embanked region has been experiencing land subsidence
176 from the beginning of polder construction in the 1960s, the annual land subsidence rate was multiplied
177 by 52 (1960-2012) to obtain an estimate of total land subsidence since polder construction.

178 Four hydrological factors were selected: precipitation, flow accumulation, Stream Power Index (SPI),
179 and Topographic Wetness Index (TWI) (Figure S2, supplementary document). To prepare the annual
180 mean precipitation layer, 10-day gridded precipitation data from 1948-2012 was collected from the
181 Bangladesh Meteorological Department (BMD). Flow accumulation, SPI, and TWI explain the
182 characteristics of natural drainage. The flow accumulation layer was obtained from the DEM in GIS by
183 deriving a continuous drainage network (Planchon and Darboux, 2002). Then, a flow direction raster
184 was obtained, applying a single-direction flow algorithm (D8) where one cell routed into the next
185 steepest of the eight neighbouring cells (Seibert and McGlynn, 2007). In the next step, a flow
186 accumulation grid was generated, which indicates the accumulated sums of water flowing in the down-
187 slope direction (Kabenge et al., 2017). SPI is a measure of the erosive power of surface runoff (Khosravi
188 et al., 2016). SPI estimates the rate of sediment that would transfer to natural drainage channels. Areas
189 with relatively high SPI values have a greater tendency to accumulate water (Bannari et al., 2017). TWI
190 depicts the likelihood of a surface is wet. A higher TWI value of an area indicates a greater chance that
191 the area will become wetter than the surrounding region (Bannari et al., 2017; Mojaddadi et al., 2017).
192 SPI and TWI were derived using the following equations in GIS.

$$SPI = A_s \times \tan \beta \quad (1)$$

193

$$TWI = \ln \left(\frac{A_s}{\beta} \right) \quad (2)$$

194 where, A_s and β indicates the specific catchment area (m^2/m) and slope gradient respectively (Khosravi
195 et al., 2016; Regmi et al., 2010; Tehrany et al., 2014b).

196 Land use affects the rate of evapotranspiration and terrain infiltration, which are essential indicators
197 determining the extent and speed of runoff (Kabenge et al., 2017; Tehrany et al., 2019b; Thornthwaite
198 and Mather, 1957). Land use data that was collected for this research included thirteen classes (Figure
199 S3 (a), supplementary document). The geological factors included topsoil texture and soil permeability
200 (Figure S3 (b) and (c), supplementary document), which also explain the level of infiltration. For
201 instance, clay lowers the infiltration rate amplifying surface runoff (Bonacci et al., 2006). Generally,
202 the characteristics of soil and land use determine the water balance of an area (Thornthwaite and Mather,
203 1957). Polders are accompanied by drainage channels and sluice gates to impede saltwater intrusion in
204 the dry season, drain excessive rainwater, and allow fresh river water flow to polders in the wet season
205 for irrigation purposes (Adnan et al., 2019b). However, the construction of polders has reduced the tidal
206 prism, promoting sedimentation in tidal channels and infilled them (Wilson et al., 2017). Inadequate
207 drainage systems in the south western region increased inundation during historical pluvial flood events
208 (Adnan et al., 2019b). In the current study, data on the existing drainage network was collected from
209 Adnan et al. (2019b) who identified drainage channels from a high-resolution satellite image. Finally,
210 two layers were created showing the distance of a given area from adjacent drainage channels and rivers
211 in GIS, applying a Euclidean distance algorithm (Figure S3 (d) and (e), supplementary document).

212

213 **2.4. Flood susceptibility modelling**

214 A spatial regression model was developed for flood susceptibility mapping, applying an ensemble of
215 bivariate frequency ratio (FR) and multivariate logistic regression (LR) models. Recent studies have
216 followed different approaches to model flood susceptibility such as weight of evidence (Khosravi et al.,
217 2016; Tehrany et al., 2014b; Tehrany et al., 2017), decision tree (DT) (Tehrany et al., 2019a), support
218 vector machine (SVM) (Mojaddadi et al., 2017; Tehrany et al., 2019a; Tehrany et al., 2014b), FR
219 (Khosravi et al., 2016; Mojaddadi et al., 2017; Tehrany et al., 2017), analytical hierarchy process (AHP)
220 (Kabenge et al., 2017; Khosravi et al., 2016), LR (Pradhan, 2010; Tehrany et al., 2014a), and artificial
221 neural networks (ANNs) (Kia et al., 2012). An ensemble of FR and LR models was applied for the
222 following reasons: i) model development is less complex compared to different machine learning
223 techniques, such as ANN, DT, and SVM (Tehrany et al., 2019b); ii) the results of FR model are easy to
224 comprehend (Khosravi et al., 2016); iii) using an ensemble of two models reduces variance-error and

225 improves prediction accuracy (Althuwaynee et al., 2014); iv) it could potentially eliminate individual
 226 bias that the expert opinion-based AHP method is likely to produce, as AHP is based on pair-wise
 227 comparisons by experts (Althuwaynee et al., 2014; Tehrany et al., 2014a); v) LR can perform regression
 228 with independent variables with continuous and/or discrete type data (Althuwaynee et al., 2014); vi)
 229 LR can estimate the probability of occurrence of dependent variables (Bubeck et al., 2013).

230 **2.4.1. Multi-collinearity diagnosis and optimizing flood conditioning factors**

231 The selected flood conditioning factors could be subject to multi-collinearity, therefore, variance
 232 inflation factors (VIF) (Midi et al., 2010) of 14 selected flood condition factors were estimated using R
 233 (Fox et al., 2018), to eliminate the factors susceptible to multi-collinearity. VIF determines the degree
 234 of variance, indicating whether coefficients are inflated by multicollinearity. VIF of a variable
 235 exceeding 2.5 creates a concern for the model, while a value ≥ 10 indicates the presence of
 236 multicollinearity (Midi et al., 2010). Twelve flood conditioning factors with a VIF value ≤ 2.5 (Bai et
 237 al., 2011) were selected for modelling flood susceptibility (Table S3, supplementary document).

238 **2.4.2. Frequency ratio (FR) model**

239 The FR model aimed to measure the influence of each class in different flood conditioning factors on
 240 flood occurrence. A FR value greater or less than 1 indicates a strong or weak correlation of a factor
 241 class with the occurrence of flooding, respectively (Khosravi et al., 2016). For a flood conditioning
 242 factor, the FR was estimated using the following equation (Khosravi et al., 2016).

$$FR = \left[\frac{N_{pix}(SX_i)}{\sum_{i=1}^n N_{pix}(SX_i)} \right] / \left[\frac{N_{pix}(X_i)}{\sum_{i=1}^n N_{pix}(X_i)} \right] \quad (3)$$

243

244 where $N_{pix}(SX_i)$ denotes the number of training flood pixels within i^{th} class of independent variable X ,
 245 $N_{pix}(X_i)$ is the total number of pixels within i^{th} class of independent variable X , and n is the total number
 246 of classes under variable X .

247 **2.4.3. Logistic regression (LR) model**

248 The statistical approach of flood susceptibility modelling assumes that the potential (probability of
 249 occurrence) of future flooding areas will be comparable to the frequency and extent of historical floods
 250 (Pradhan, 2010). The LR model incorporated 700 training flood observation data (flood and non-flood)
 251 as a dependent variable and 12 flood conditioning factors as independent variables. A weight to each
 252 cell in different flood conditioning factors was provided according to estimated FR, before
 253 incorporating them into the LR model (Althuwaynee et al., 2014; Tehrany et al., 2014a). The training
 254 flood observation data was used to extract the value of FR of 12 flood conditioning factors in GIS. Then
 255 regression coefficients and p-statistics of each variable as well as the coefficient of determinants (R^2)

256 of the model were estimated using the ‘mlogit’ package in R (Croissant and Croissant, 2018). The
 257 obtained regression coefficients were incorporated in equation (4) (Tehrany et al., 2014a) in GIS to
 258 derive the probability (p) of flood occurrence in the study area.

$$p = 1/(1 + e^{-z}) \quad (4)$$

259 where p is the probability of an event occurring. In the present situation, p is the estimated annual
 260 probability of flooding, indicating the likelihood of a cell being inundated annually, for a similar set of
 261 flood conditioning factors explicating inundated areas during the historical events; z is the linear
 262 combination of independent variables, which was estimated using the following equation.

$$z = b_0 + b_1x_1 + b_2x_2 + \dots + b_nx_n \quad (5)$$

263 where b_0 is the model intercept, b_i ($i = 1, 2, \dots, n$) indicates the regression coefficients of independent
 264 variables, and x_i ($i = 1, 2, \dots, n$) represents the FR of n number of independent variables (Table 2).
 265 Obtained flood probability index map was categorized into five equal classes, representing different
 266 categories of flood susceptible zones. Besides, a cut-off flood probability value was optimised so that
 267 areas with flood probability above the cut-off value were classified as flood susceptible zones, and vice
 268 versa. The method used to optimize cut-off flood probability value is explained in Section 2.4.4.

269 **2.4.4. Sensitivity analysis and model validation**

270 The flood susceptibility model validation was performed using a well-known method called receiver
 271 operating characteristic (ROC) curve and subsequent area under the curve (AUC) (Althuwaynee et al.,
 272 2014; Arabameri et al., 2019; Khosravi et al., 2016; Tehrany et al., 2014a). ROC values express the
 273 ability of the model to correctly separate positive and negative observations in the validation samples
 274 (Arabameri et al., 2019). To develop this plot, the estimated annual flood probability values of all cells
 275 were sorted in descending order. Then the ordered flood probability index map was classified into 100
 276 categories, with cumulative 1% (0.01) break. The resultant 100 categories of the probability index were
 277 plotted on the x-axis, which represents false-positive rates of annual flood probability. Then observed
 278 flood points were overlaid on the flood probability index map. The cumulative relative frequency of
 279 observed flood points (true positive rate) was plotted against each category of false-positive rate
 280 (Tehrany et al., 2019b).

281 The AUC is a global accuracy statistic, where the thresholds range from 0 (random prediction) to 1
 282 (perfect prediction): Excellent (0.9–1), very good (0.8–0.9), good (0.7–0.8), moderate (0.6–0.7) and
 283 weak (<0.6) (Arabameri et al., 2019). AUC values estimated by using training and test data indicate the
 284 success and prediction accuracy of the model, respectively (Tehrany et al., 2019b). Moreover, observed
 285 relative flood frequency in each test flood location was plotted against corresponding modelled annual
 286 flood probability value and a third-degree polynomial regression model was established.

287 The values of various statistical indices such as overall accuracy, specificity, sensitivity, positive
 288 predictive value, negative predictive value (Tehrany et al., 2019b), and kappa statistic (McHugh, 2012)
 289 were estimated to measure the comparative performance of each model. Thus, modelled flood
 290 probability index values of all observed flood points (training and test) were binarized, optimizing a
 291 cut-off flood probability value using the ‘OptimalCutpoints’ package in R, which is “the optimal point
 292 on the ROC curve closest to the point (0, 1)” (López-Ratón et al., 2014).

293 **2.5. Analysing the impact of TRM on flooding**

294 **2.5.1. *Simulating sediment deposition in selected TRM sites***

295 To model sediment deposition during the operation of TRM, suitable ‘beels’ were identified. ‘Beels’
 296 were delineated using a DEM-based flood routing model (Diaz-Nieto et al., 2011), established for the
 297 south western embanked region by Adnan et al. (2019b). A total of 234 ‘beels’ were identified within
 298 the embanked region, with sizes ranging from 0.74km² to 48.53km² (Figure 5 (a)). A GIS-based
 299 suitability analysis was performed to select TRM sites. First, indicators to perform suitability analysis
 300 were selected. Whilst limited information is available on indicators to select TRM sites, Masud et al.
 301 (2018) proposed a Sustainability Index of TRM (SITRM), conceptualizing the spatial and temporal
 302 impact of TRM based on a characterisation of the tidal river, environment, resilience, floodplain
 303 ecosystem, human health, and community. To identify suitable TRM sites, five indicators were selected:
 304 i) tidal prism; ii) river salinity; iii) flood prone areas; iv) crop production; and v) size of the ‘beel’. These
 305 indicators are associated with the tidal river, environment, resilience, and floodplain ecosystem
 306 components of SITRM. The suitability analysis did not include indicators related to human health and
 307 community, due to unavailability of required spatial data for the entire study area.

308 The inter-tidal volume or tidal prism (P) explains the availability of tidal flow required to implement
 309 TRM. A higher P indicates an adequate tidal flow for TRM, given that water carries the required amount
 310 of sediment (Talchabhadel et al., 2018). The study area is comprised of lands from 46 river sub-basins
 311 and P was approximated in individual sub-basin using the following equation (Lakhan, 2003):

$$P = HA \quad (6)$$

312 where H is the tidal range and A is the surface area of each sub-basin. This is an approximation in basins
 313 where the inter-tidal area is significant relative to the overall surface area, but as the bathymetric form
 314 through the delta is rather similar, we do not expect this approximation to bias the results. Sub-basins
 315 were generated in GIS incorporating river outlet location data collected from BWDB, who also provided
 316 daily tidal water level data for each outlet. The difference between the mean water level in each outlet
 317 during the high and low tide is the tidal range.

318 Salinity is an important indicator of floodplain ecosystems. TRM operation allows river water to enter
 319 a tidal plain twice a day. A high concentration of salinity in tidal river water will cause an increase in

320 soil salinity, making land unsuitable for crop production (Masud et al., 2018). Therefore, the level of
 321 river salinity is inversely correlated with the suitability of a site to operate TRM. Monthly observed
 322 river salinity data in each outlet of river sub-basins was collected from the BWDB, which was averaged
 323 across the year, where salinity level ranged from 0.23dS/cm to 12.39dS/cm (Figure S9 (b),
 324 supplementary document). Since TRM primarily intends to minimize flooding problems, ‘beels’ that
 325 were frequently affected by flooding are more suitable for TRM. Hence, mean flood frequency in each
 326 ‘beel’ was estimated from the developed flood inventory map (Figure S9 (a), supplementary document).
 327 As, TRM primarily aims to increase crop production in flood-prone areas (Gain and Schwab, 2012),
 328 hence ‘beels’ with land used for agriculture are the most suitable TRM sites. Besides, relatively smaller
 329 ‘beels’ are more suitable for TRM implementation, which makes stakeholders engagement less complex
 330 (Masud et al., 2018).

331 A rank (y) was assigned to each ‘beel’ according to the level of suitability in a 1 (very low) to 5 (very
 332 high) scale, in relation to the value of each suitability parameter (x). Ranks were estimated applying a
 333 linear interpolation technique proposed by Davis (2002). If the value of a parameter is positively
 334 correlated with the level of suitability for a TRM site, then Equation 7 was used, otherwise, Equation 8
 335 was applied (Adnan et al., 2019a). For land use data, a dummy code was provided to each land use
 336 class, based on subjective judgement (Abdullah et al., 2018). Three main categories of land use such as
 337 agriculture, mixed agriculture and aquaculture, and aquaculture were given codes of 3, 2, and 1,
 338 respectively.

339

$$\text{If } y \propto x, \quad y'_n = \frac{(y_2 - y_1)(x'_n - x_{min})}{(x_{max} - x_{min})} + y_1 \quad (7)$$

$$\text{If } y \propto \frac{1}{x}, \quad y'_n = \frac{(y_2 - y_1)(x'_n - x_{max})}{(x_{min} - x_{max})} + y_1 \quad (8)$$

340 where y'_n is the suitability rank of a parameter for the n^{th} ‘beel’ ($n = 1, 2, 3, \dots, 234$); the maximum
 341 rank $y_2 = 5$; minimum rank $y_1 = 1$; x'_n is the value of a parameter for the n^{th} ‘beel’; x_{max} is the maximum
 342 value of a parameter among all ‘beels’, and x_{min} is the minimum value of a parameter among all ‘beels’.

343 Simulated sediment deposition data were collected from Talchabhadel et al. (2018) for five ‘beels’
 344 located in Polder 24 (Figure 1 (c)). Talchabhadel et al. (2018) simulated sediment deposition in TRM
 345 sites based on a two-dimensional (2D) numerical model, established through laboratory flume
 346 experiments to understand the mechanism of sediment transportation and deposition. During the
 347 experiment, a constant discharge of 5.1 l/s as upstream river flow and 2.8 l/s as downstream tidal flow
 348 were provided. To represent high and low tidal flow, the adjustable gate was used. The gate was kept
 349 closed for 2 minutes to represent high tide, when the downstream flow from water pump was supplied

350 along with dry sediment, of mean diameter equal to 94 μm and density 2.65 g/cc, from a sediment
351 feeder. Then, the gate was opened for the next 2 minutes, when the downstream supply of water and
352 sediment were stopped, representing a low tide. Thus, a total of 8 minutes of experiments were
353 performed to represent two complete tidal cycles in a day, as is the case in the coastal region of
354 Bangladesh. The study assessed the optimum size of the link canals and the importance of constructing
355 cofferdams in the river upstream of the opening for effective sediment deposition around the attached
356 tidal basin. To make the study less complicated, the experimental setup involved a straight river and
357 tidal basin attached in a perpendicular alignment. Photogrammetric techniques were applied to measure
358 the deposited sediment along with a laser displacement sensor (Figure S4-S7, supplementary
359 document).

360 The 2D numerical model was developed based on the shallow water flow equations and suspended
361 sediment transport. The model was applied to explore the efficacy of the land heightening of the tidal
362 basin with changing discharges and opening sizes. The numerical models were tested in different
363 scenarios and compared with experimental results. The model reproduced the water depth and velocity
364 reasonably well (percentage bias = $\pm 5\%$ and coefficient of determination ≥ 0.7). Suspended sediment
365 concentration (SSC) and the deposited sediment were also replicated in good agreement with
366 experimentally measured data. The surface was divided by an unstructured mesh using the GID
367 software developed by the International Center for Numerical Methods in Engineering (CIMNE)
368 (<https://www.gidhome.com>). A DEM of 5m resolution was derived from the bathymetric data of March
369 2007 provided by the Institute of Water Modelling (IWM) Bangladesh. A Manning roughness
370 coefficient of 0.025 was assigned to meshes covering the river system, channels, and connecting canals,
371 whereas a Manning roughness coefficient of 0.04 was provided in remaining areas. Simulated sediment
372 deposition during six months of TRM implementation in 'beel' Khukshia (*beel-2*, Figure 5 (b)) was
373 further validated against observed sediment depth at various locations, collected through field-work in
374 November 2012. Further details on the experimental setup, model development can be found in
375 Talchabhadel et al. (2017) and Talchabhadel et al. (2018).

376 River bathymetry and measured sediment concentration data are not available for the whole area under
377 study. Therefore, based on the simulated sediment deposition in five 'beels', sediment deposition in
378 remaining 'beels' was parameterised, developing an ordinary least square (OLS) regression in GIS. The
379 OLS model included pixelwise height of the deposited sediment as dependent variable and factors
380 explaining the deposition of sediment as independent variables. Five geomorphological variables were
381 identified that explained the height of the deposited sediment in each pixel: i) land elevation (E_l); ii)
382 distance from drainage (link canal) (D_d); iii) TWI; iv) slope (S_l); and v) curvature (C). Figure S1-Figure
383 S3 in the supplementary document show these variables. The estimated intercept and regression
384 coefficients were used to form the Equation 9, which was applied to simulate sediment deposition in
385 remaining suitable 'beels'.

$$\text{Sediment deposition (m)} = 1.73 - 0.13E_l - 0.13D_a - 0.04 TWI - 0.03S_l + 0.04C \quad (9)$$

386

387 Validation of the developed OLS regression model was performed plotting the parameterized pixelwise
388 sediment height in five ‘beels’ against the obtained modelled sediment height and estimating the R^2
389 value of 0.88 (Figure S8, supplementary document).

390 **2.5.2. Estimating the impact of TRM on flooding**

391 The change in land elevation and flood susceptibility for pre- and post-TRM implementation scenarios
392 was compared. TRM has already been implemented in five ‘beels’ within Polder 24 (ADB, 2007),
393 where simulation of sediment deposition was performed. A 50m resolution DEM was collected from
394 IWM, which was developed from a toposheet map (1:20000) produced by Survey of Bangladesh (SoB)
395 in 1990-1991, carrying out an aerial photography survey. The IWM and ALOS DEMs were used to
396 estimate observed land elevation in pre-TRM and post-TRM scenarios in five ‘beels’, respectively.
397 Because the TRM operations within these areas were interrupted before full sediment accumulation
398 could occur, in practice land accretion was much lower than expected. In these cases, the sediment
399 deposition was modelled for the remainder of the implementation period (1 to 5-year) to estimate the
400 potential sediment accumulation during a 5-year implementation. Finally, the observed and modelled
401 increase in land elevation were compared after the implementation of TRM.

402 A change in land elevation due to the implementation of TRM promoted changes in four other flood
403 conditioning factors: aspect, slope, curvature, and Stream Power Index (SPI). Since TRM intended to
404 alleviate land subsidence, hence the value of this factor was considered as zero for the post-TRM
405 scenario. Parameterized sediment deposition was added to the existing ALOS DEM to develop DEM
406 for the post-TRM scenario. Following the similar procedure explained in Section 2.4, flood
407 susceptibility at post-TRM scenario was estimated.

408 **3. Results and discussion**

409 **3.1. Delineation of flood susceptible zones**

410 **3.1.1. The outcome of the FR model**

411 Table 1 summarizes the outcome of the FR model, showing the relationship between the flood
412 conditioning factors and flooding. Areas with lower elevation and slope as well as curvature with flat
413 and concave characteristics were prone to flooding. Regarding aspect, cells facing east, west, and
414 northwest as well as flat areas were highly susceptible to flooding. A greater percentage of flood
415 locations were found in areas where relatively higher level land subsidence occurred.

416 Table 1: Spatial relationship between flood locations and flood conditioning factors

Variables	Class	Frequency ratio (FR)	Variables	Class	Frequency ratio (FR)
Aspect	Flat (-1)	1.45	Land uses	Shrimp culture	0.93

Variables	Class	Frequency ratio (FR)	Variables	Class	Frequency ratio (FR)
	North (0-22.5)	0.84		Rice field	1.03
	Northeast (22.5-67.5)	0.92		Mixed rice field, shrimp, and other fish culture	3.52
	East (67.5-112.5)	1.00		Mangrove	0
	Southeast (112.5-157.5)	0.80		Shrimp and other fish culture	3.40
	South (157.5-202.5)	0.77		Other crop agriculture land	0.55
	Southwest (202.5-247.5)	0.95		Freshwater fish culture	1.41
	West (247.5-292.5)	1.02		River/Canal	1.26
	Northwest (292.5-337.5)	1.32		Settlement with Homestead Vegetation (Rural)	0.35
	North (337.5-360)	0.91		Settlement with Homestead Vegetation (Urban)	0.46
				Water Body	0
				Others	0
Elevation (m)	≤ 0	1.50	Soil texture	Silty clay and silty clay loam	1.78
	0 - 1	1.34		Clay	3.54
	1 - 2	1.29		Silty clay	0.88
	2 - 3	1.30		Silt loam and Silty clay	0.38
	3 - 4	0.98		Unclassified	0.96
	4 - 5	0.68		Silt loam	0.61
	5 - 7	0.25			
	7 - 9	0.15		Silty clay and clay	1.34
	> 9	0		Silt loam and clay	1.02
Slope (degree)	0 – 0.44	1.52		Silty clay loam and silty clay	0.86
	0.44 - 0.66	1.23		Silty clay loam and silt loam	0.43
	0.66 – 0.88	1.09		Silty clay loam	0
	0.88 - 1.09	1.15			
	1.09 - 1.32	0.84			
	1.32 - 1.98	1.09			
	1.98 - 2.64	0.78			
	2.64 - 3.73	0.69			
	3.73 – 56.01	0.38			
Curvature	Convex	0.98	Soil permeability	Moderate	0.58
	Flat	1.06		Mostly moderate	1.21
	Concave	1.00		Slow	1.25
Land subsidence (m)	< 0.12	0.32		Unclassified	0.96
	0.12 - 0.16	0.15		Mostly slow with some Moderate	0.39
	0.16 - 0.20	1.47		Mostly moderate with some slow	0.38
	0.20 - 0.23	1.95		Mostly slow	0.64
	0.23 - 0.25	1.17			
	0.25 - 0.26	1.15			
	0.26 - 0.265	0.83			
	0.265 - 0.27	0.69			
	> 0.27	1.31			
Precipitation (mm)	1593 - 1645	1.18	Distance from drainage channels (m)	0 - 90	0.93
	1646 - 1706	1.64		90 - 192.09	0.82
	1707 - 1766	1.06		192.09 - 308.87	1.17
	1767 - 1806	1.00		308.87 - 445.98	0.87

Variables	Class	Frequency ratio (FR)	Variables	Class	Frequency ratio (FR)
	1807 - 1863	1.20		445.98 - 607.45	1.10
	1864 - 1903	0.71		607.45 - 831.93	1.17
	1904 - 1948	1.10		831.93 - 1176.52	0.95
	1949 - 2178	1.04		1176.52 - 2012.01	0.92
	2179 - 2621	0.09		2012.01 - 13232.18	1.30
Stream power index (SPI)	-13.82 to -10.93	0.91	Distance from rivers (m)	0 - 180	0.89
	-10.93 to -10.19	1.05		180 - 450	0.95
	-10.19 to -7.02	0.40		450 - 780	0.84
	-7.02 to -3.48	1.30		780 - 1168.46	0.68
	-3.48 to -2.74	1.14		1168.46 - 1636.85	0.68
	-2.74 to -1.99	0.84		1636.85 - 2248.4	0.92
	-1.99 to -1.16	1.06		2248.4 - 3100.61	1.26
	-1.16 to 0.05	1.08		3100.61 - 4477.95	1.49
	0.05 to 10.01	1.32		4477.95 - 12559.4	1.18

417 Areas characterized by higher values of SPI contained a greater number of floods. Floods occurred
 418 primarily in areas that were used mostly for agricultural and aquaculture purposes, compared to
 419 settlement areas where a relatively lower number of flood locations were found. In relation to soil
 420 texture, four categories of soils contained most of the flood locations: 'silty clay and silty clay loam',
 421 'clay', 'silty clay and clay', and 'silty clay loam and silty clay' type soil. Areas with 'moderate' or
 422 'slow' permeable soils are prone to flooding. Besides, floods are more likely to occur in areas away
 423 from adjacent rivers, as water is difficult to drain from those areas.

424 3.1.2. The outcome of the LR model

425 Table 2 summarizes the outcome of the LR model. Among the 12 factors, six were statistically
 426 significant (p -value ≤ 0.05). The flood probability index map derived in this study is shown in Figure 2
 427 (b). The optimization of flood probability values at observed flood locations yielded a cut-off (minimum
 428 threshold probability) value of 0.6. A major portion of the study area is susceptible to flooding, which
 429 was mostly inundated during different historical flood events (Figure 2 (a)). The annual probability of
 430 flooding in 48% of the studied area is ≥ 0.8 , where observed mean relative flood frequency is 0.2. This
 431 result indicates that inundations occurred during four historical flood events, on average, as the
 432 maximum frequency of inundation was 20 in a total of 25 observation years (Figure S9 (a),
 433 Supplementary document).

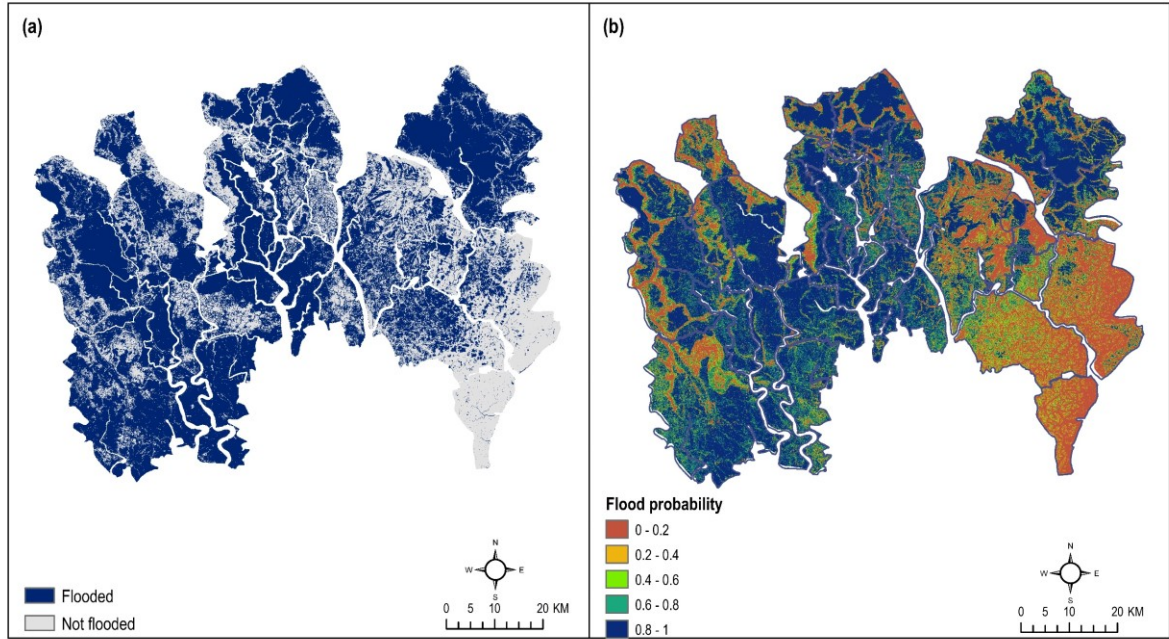
434 Table 2: Logistic regression model to predict the occurrence or not occurrence of floods

Variables	Coefficient	Standard error	p -value
Intercept	-36.328	6.957	$1.778 e^{-07}$ ***
Aspect (A_s)	0.023	0.008	0.003 **
Elevation (E_l)	0.045	0.004	$< 2.2e^{-16}$ ***
Slope (S_l)	-0.008	0.006	0.208
Curvature (C)	0.244	0.067	0.0002 ***
Land subsidence (L_s)	0.004	0.003	0.006 **
Precipitation (P)	0.008	0.005	0.087 ▫
SPI	0.003	0.007	0.614
Land use (L_u)	0.011	0.001	$8.221e^{-10}$ ***
Soil texture (S_t)	0.011	0.004	0.099 ▫
Soil permeability (S_p)	0.008	0.005	0.003 **

Distance from drainage channels (D_d)	0.011	0.010	0.372
Distance from rivers (R_d)	0.008	0.006	0.112

R^2 : 0.77; Significance codes: 0 '***' 0.001 '**' 0.01 '*' 0.05 '.' 0.1 ' ' 1

435
436



437
438
439

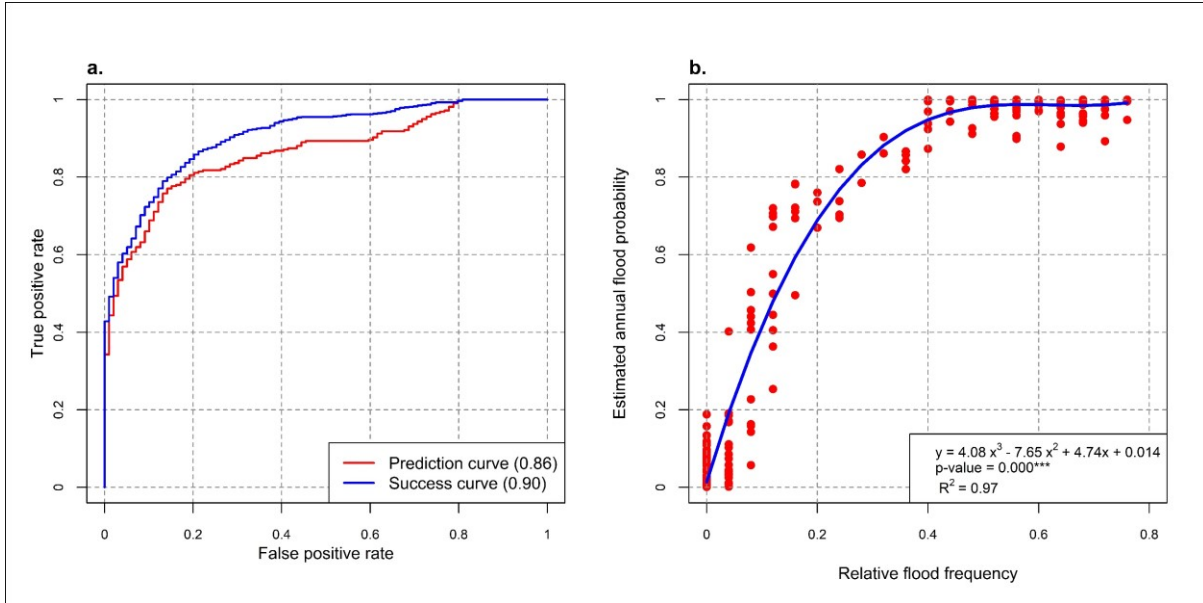
Figure 2: (a) Extent of inundation during floods from 1988-2012 (b) Annual flood probability index map

440

441 **3.1.3. Model validation**

442 The estimated AUC for test dataset was 0.86, which indicates a ‘very good’ prediction accuracy. In
 443 addition, the AUC of 0.90 for the training dataset implies an ‘excellent’ success rate of the model
 444 (Figure 3 (a)). Figure 3 (b) shows how the estimated flood probability increased with observed relative
 445 flood frequency. A third-degree polynomial equation was generated that explains the type of
 446 relationship between observed relative flood frequency and modelled flood probability. The general
 447 goodness of fit of this equation is verified by the estimated R^2 value of 0.97.

448



449

450 Figure 3: (a) ROC curve to validate flood probability map (b) Relative flood frequency and estimated
 451 annual flood probability of test flood observation points

452 Moreover, an overall accuracy of 93% explains the percentage agreement of pixels correctly classified.
 453 The Kappa coefficient of 0.85 indicates ‘almost perfect’ agreements between observed and modelled
 454 flood locations (Table 3).

455

Table 3: Validation of flood susceptibility model

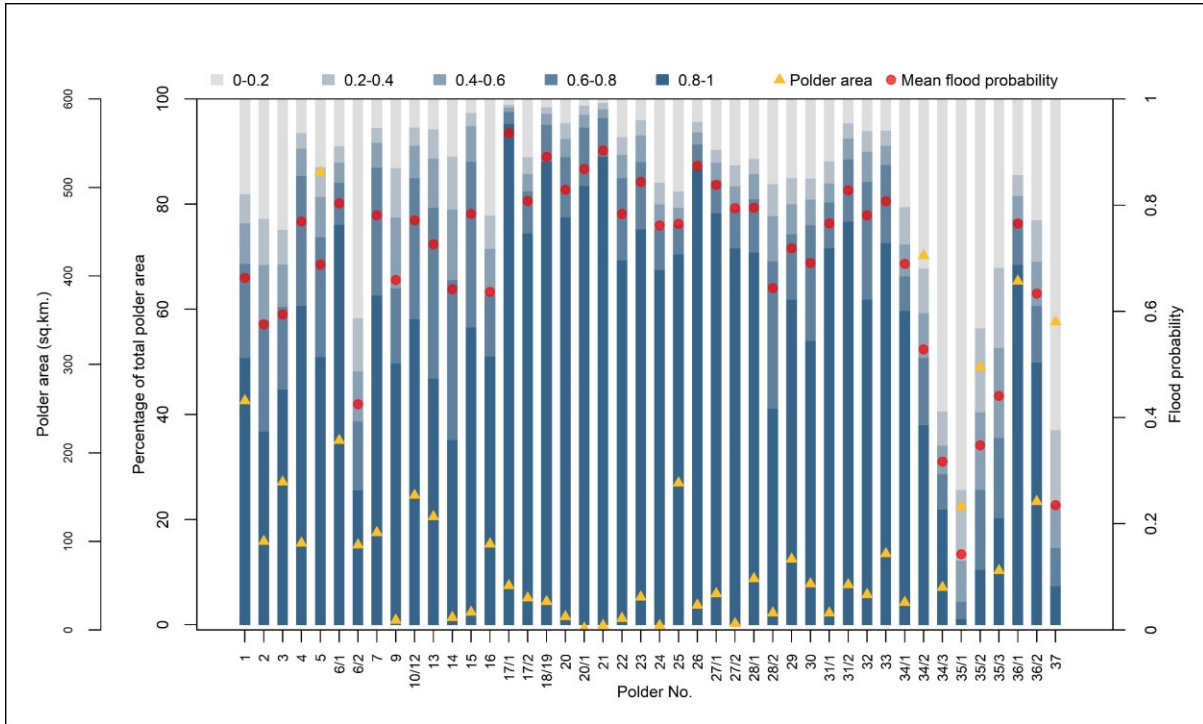
Statistical index parameters	Values
True positive (correctly classified flood locations)	546
True negative (correctly classified non-flood locations)	381
False positive (incorrectly classified flood locations)	33
False negative (incorrectly classified non-flood locations)	40
Positive predictive value (PPV) (%)	95
Negative predictive value (NPV) (%)	90
Sensitivity (%)	93
Specificity (%)	92
Overall accuracy (%)	93
Kappa statistic	0.85

456

457 **3.1.4. Characteristics of flood susceptible region**

458 Since the average flood probability in most of the polders is greater than the minimum threshold flood
 459 probability, the major portion of the region is classified as being susceptible to flooding annually. More
 460 than 50% of the total area across 30 polders has an annual flood probability value ≥ 0.8 (Figure 4). The

461 major proportion of agricultural and aquaculture land use is located within flood susceptible zones (65%
 462 and 81%, respectively). More than 90% of the area under mixed agriculture and aquaculture land use is
 463 susceptible to flooding. A substantial proportion of people (44.5%) live in a relatively small proportion
 464 (22.8%) of settlement areas, which are susceptible to flooding (Table S4, supplementary document).
 465



466

467 Figure 4: Ratio of flood susceptible lands in various polders

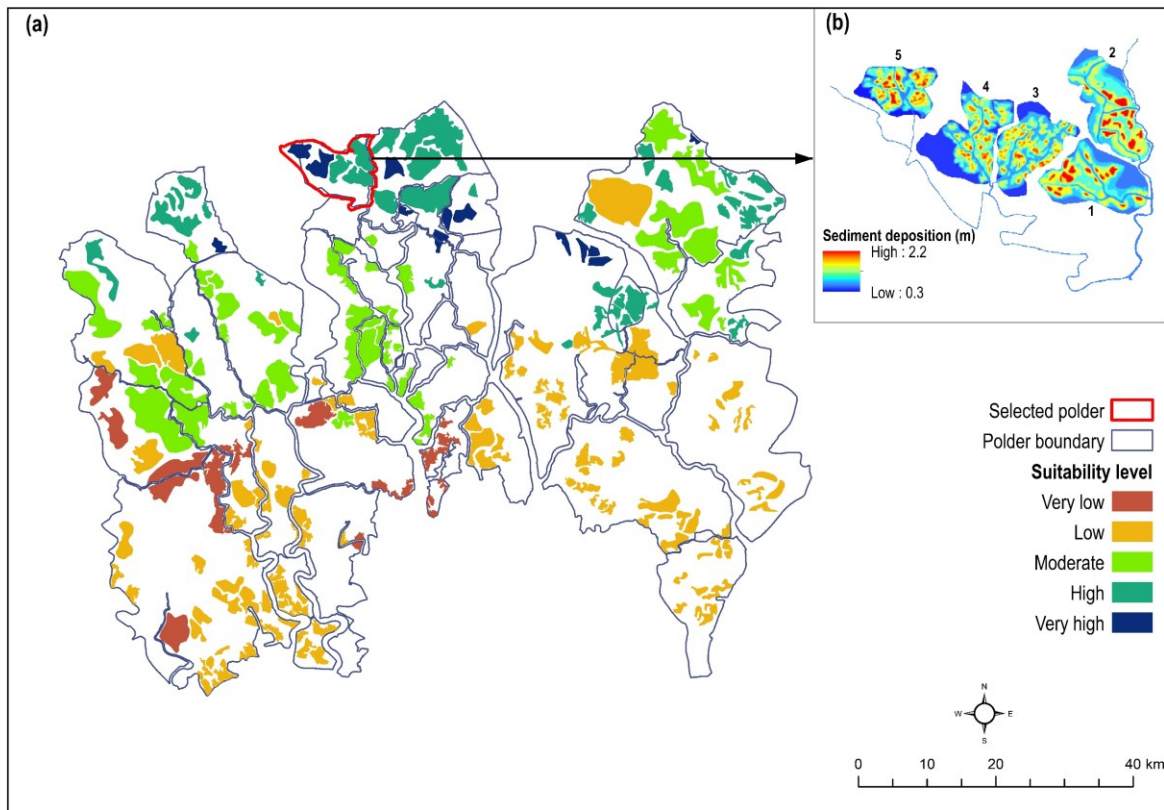
468

469 **3.2. Impact of TRM in reducing flood susceptibility**

3.2.1. Sediment deposition and restoring land elevation

470 The suitability analysis yielded 106 ‘beels’ that are suitable (estimated suitability rank from 3
 471 (moderate) to 5 (very high)) to operate TRM. Most of the polders in the northern segment of the study
 472 region are suitable, since these areas are highly prone to flooding and where most of the agricultural
 473 activities take place, and the salinity level in surrounding rivers is relatively lower (Figure 5 (a)). The
 474 result of the sediment transportation and deposition model indicated that continuous operation of TRM
 475 in sample ‘beels’ could reclaim a maximum of 1.4m land elevation in 5 years (Figure 5 (b)).

476

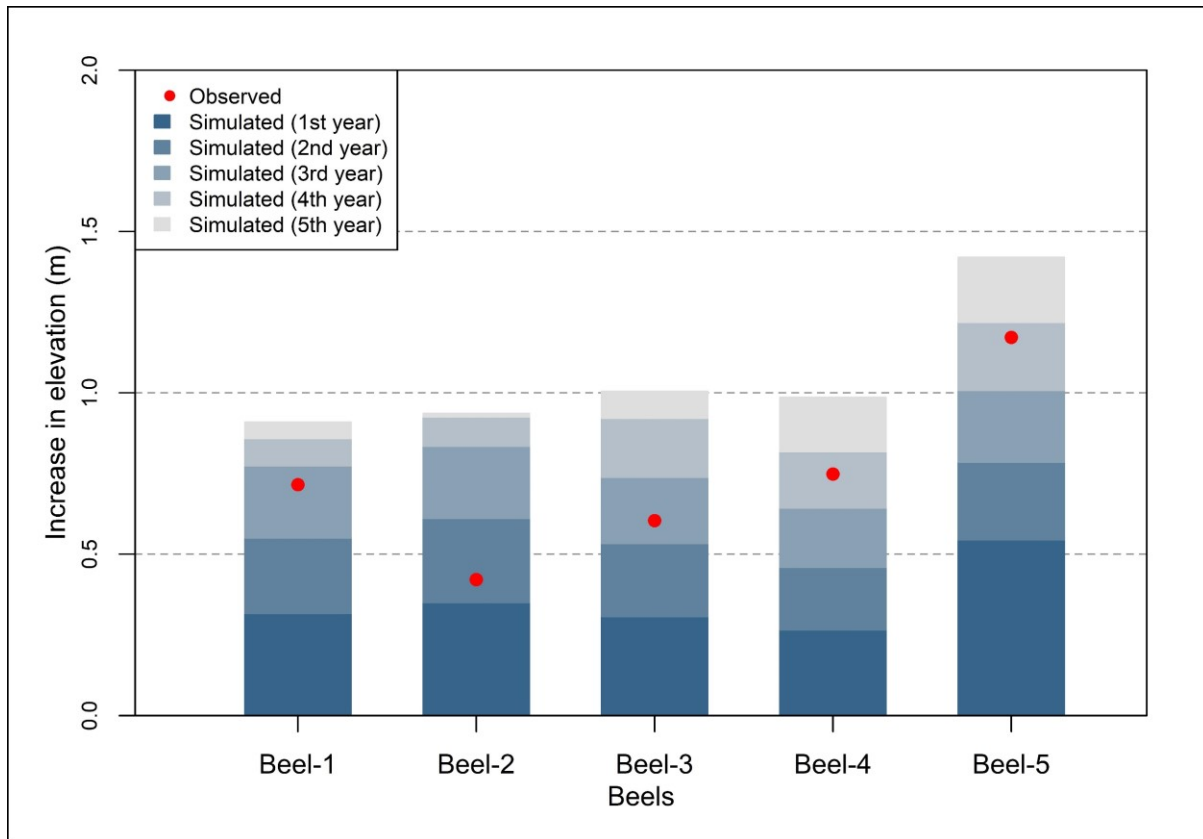


477

478 Figure 5: (a) Suitable 'beels' for TRM implementation; (b) sediment deposition in selected 'beels'

479 Figure 6 exhibits the extent to which TRM has been able to alter land elevation in five 'beels' in Polder
 480 24. It also shows the land elevation that uninterrupted TRM might have recovered to in the five-year
 481 operation time. The mean elevation in all five 'beels' increased as a result of TRM (observed),
 482 implemented for various time steps. For instance, the length of TRM operation period in *beel-1* (Beel
 483 Bhaina) was four years (1997-2001), whereas disruption in *beel-2* ('Beel' Khukshia) caused an
 484 extended implementation period of six years (2006-2012). Results from the sediment transportation and
 485 deposition model indicated that an uninterrupted and planned implementation (e.g., construction of link
 486 canals, rotation of openings) of TRM might have led to a further increase in land elevation than which
 487 has been achieved. For instance, the three-year implementation of TRM in *beel-1* might have recovered
 488 a similar depth of sediment that deposited in four years in practice. However, *beel-2* is an example of
 489 an unsuccessful TRM, where interruptions occurred throughout the implementation period. The
 490 observed depth of sediment deposition in six years was similar to the estimated depth of sedimentation
 491 obtained after two years of TRM implementation. The analysis noted that TRM was the most successful
 492 in *beel-5*, as it yielded the highest depth of sediments.

493



494

Figure 6: Change of land elevation in five selected 'beels' after implementing TRM

495

496

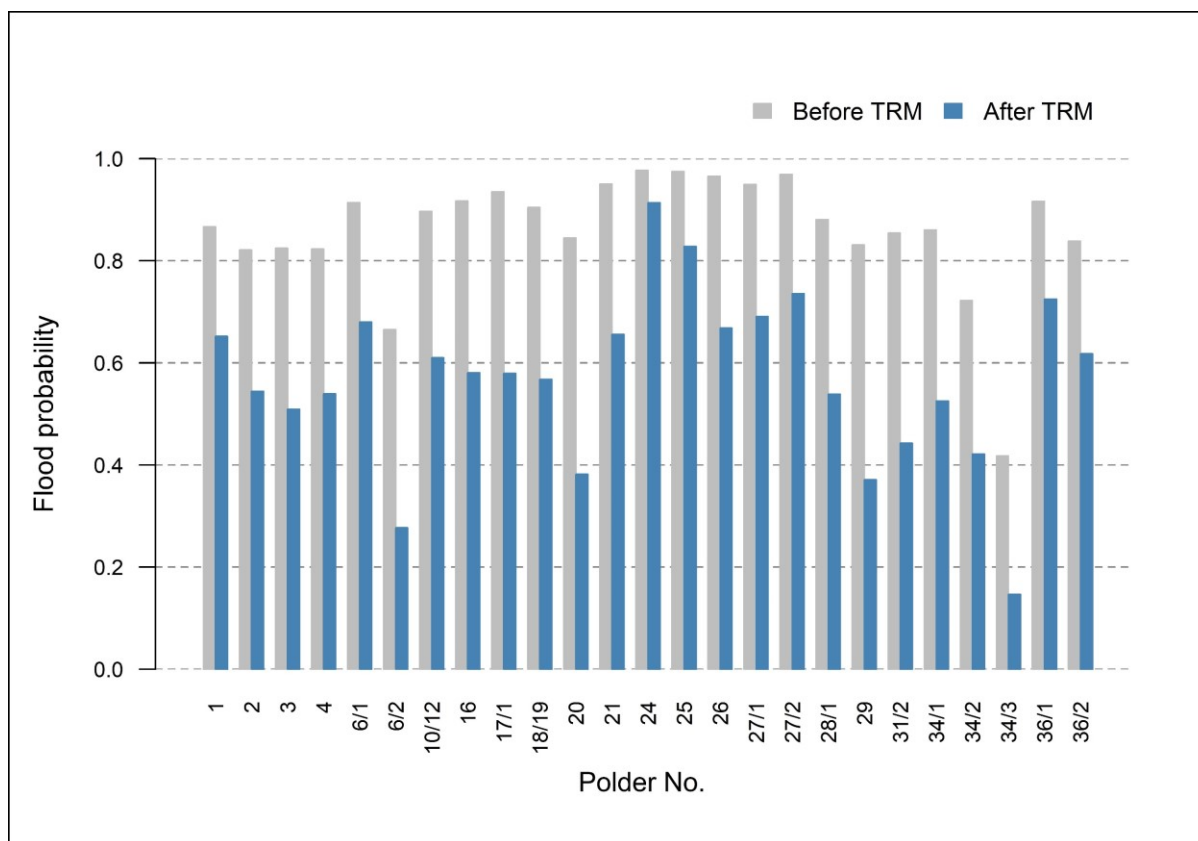
3.2.2. Flood susceptibility before and after TRM implementation

497

498 The application of TRM is predicted to reduce the annual probability of flooding from 0.86 (on average)
 499 to 0.57 (on average), in 106 suitable 'beels' located within 25 polders (Figure 7). A reduction of annual
 500 probability of flooding resulted from a change of various geomorphological flood-inducing factors.
 501 Along with increasing the surface elevation, the implementation of TRM could potentially improve the
 502 physical condition of natural drainage basin by reducing the value of SPI which reduces the erosion
 503 potential of the surface. Besides, changes in surface curvature would decelerate surface flow. All these
 504 changes result in a reduced annual probability of flooding in the TRM sites.

505 The implementation of TRM reduced flood susceptibility across 'beels' in 13 polders, which were
 506 susceptible to flooding before. In general, flood susceptibility in 35% of areas of the selected 'beels'
 507 reduced due to TRM. However, the impact of TRM varied across 'beels' in different polders. The
 508 maximum reduction in the annual probability of flooding was estimated in 'beels' located within Polder
 509 20 and Polder 29 (Figure 7), where the probability of flooding reduced by 0.46 on average.

510



511

512 Figure 7: Annual probability of flooding in suitable ‘beels’ in different polders before and after the
513 implementation of TRM

514 **4. Conclusion**

515 TRM in the south western coastal region of Bangladesh was implemented to promote sedimentation in
516 low-lying ‘beels’, creating an opportunity of increased agricultural production by reducing flooding. In
517 practice, the success of TRM was hampered by interruptions during its operation, primarily caused by
518 various implementation hurdles such as social unrest, conflict, and issues related to compensation. This
519 study modelled the potential effectiveness of TRM in restoring land elevation and reducing flood
520 susceptibility in the study area. A flood susceptibility model has been developed that successfully
521 predicts flooding locations based on coordination of conditioning factors, the most influential being
522 land elevation, aspect, curvature, land use, land subsidence, and soil permeability. The study identified
523 106 suitable ‘beels’ where flooding could potentially be alleviated by a change in land elevation that
524 could, in turn, be achieved by sediment deposition during TRM implementation. Sediment deposition
525 in identified ‘beels’ was parameterised based on simulated sediment data on five sample ‘beels’. Flood
526 susceptibility in those ‘beels’ was compared between pre- and post-TRM implementation scenarios.

527 The results indicated that floods in the south western embanked region primarily occurred in areas with
528 common characteristics such as low elevation and slope, flat landscape-scale curvature, high land
529 subsidence rates and SPI, and moderate to low soil permeability. The study also estimated that a major

530 portion of the total region is susceptible to flooding, being inundated during various historical flood
 531 events. Agricultural and aquaculture activities mostly take place in these flood susceptible zones. Wider
 532 implementation of TRM would result in increased land elevation, which could alleviate land subsidence
 533 and modify several geomorphological factors such as aspect, slope, curvature, and SPI. Such changes
 534 in the surface could help to reduce the probability of flooding in a range of polders. The results described
 535 here further indicate that an uninterrupted 5-year implementation of TRM might have resulted in a
 536 greater increase in land elevation (in 'beels') than has actually been achieved in practice, due to
 537 interruptions in implementation of several TRM projects.

538 Modelling sediment transportation in low-lying areas is a complex and data-intensive process. Scarcity
 539 of data, including observed sedimentation, makes it difficult to model sediment deposition
 540 hydrodynamically for the entire region. Accuracy of the flood susceptibility modelling results depends
 541 on input parameters used, particular the DEM. The ALOS DEM is considered to be the most accurate
 542 freely available DEM, which has a low root mean square error (1.78m) in vertical accuracy (Hasan et
 543 al., 2020). To address the uncertainty related to DEM accuracy, topographical and hydrological
 544 parameters were discretised into various quantile classes and incorporated to the flood susceptibility
 545 model. Relevant discretised variables were also used to parameterise sediment deposition in suitable
 546 'beels'.

547 This study attempted to assess the suitability of a site for TRM implementation mainly from the
 548 perspective of the physical environment. Socio-economic and governance considerations have proved
 549 to be critical to the successful implementation of TRM, but these have not been addressed in this study.
 550 This study shows the extent to which an uninterrupted implementation of TRM could help to alleviate
 551 flood susceptibility in the region. It further characterises polders according to the level of flood
 552 susceptibility as well as suitability to implement TRM, which could be a useful guide for national
 553 organizations like BWDB, who are responsible for managing water resources in polders.

554 **Acknowledgement**

555 This work is an output from the REACH programme (www.reachwater.org.uk) funded by UK Aid from
 556 the UK Department for International Development (DFID) for the benefit of developing countries
 557 (Aries Code 201880). However, the views expressed, and information contained in it are not necessarily
 558 those of or endorsed by DFID, which can accept no responsibility for such views or information or any
 559 reliance placed on them.

560 **5. References**

- 561 Abdullah AYM, Biswas RK, Chowdhury AI, Billah SM. Modeling soil salinity using direct and indirect
 562 measurement techniques: A comparative analysis. *Environmental Development* 2018.
 563 Abdullah AYM, Masrur A, Adnan MSG, Baky MAA, Hassan QK, Dewan A. Spatio-Temporal Patterns
 564 of Land Use/Land Cover Change in the Heterogeneous Coastal Region of Bangladesh between
 565 1990 and 2017. *Remote Sensing* 2019; 11: 790.

- 566 ADB. Bangladesh: Khulna-Jessore Drainage Rehabilitation Project - Project Performance Evaluation
567 Report. Asian Development Bank Bangladesh, 2007.
- 568 Adnan MSG, Dewan A, Zannat KE, Abdullah AYM. The use of watershed geomorphic data in flash
569 flood susceptibility zoning: a case study of the Karnaphuli and Sangu river basins of
570 Bangladesh. *Natural Hazards* 2019a; 99: 425–448.
- 571 Adnan MSG, Haque A, Hall JW. Have coastal embankments reduced flooding in Bangladesh? *Science*
572 *of the Total Environment* 2019b; 682: 405-416.
- 573 Alam MS, Sasaki N, Datta A. Waterlogging, crop damage and adaptation interventions in the coastal
574 region of Bangladesh: A perception analysis of local people. *Environmental Development*
575 2017; 23: 22-32.
- 576 Althuwaynee OF, Pradhan B, Park HJ, Lee JH. A novel ensemble bivariate statistical evidential belief
577 function with knowledge-based analytical hierarchy process and multivariate statistical logistic
578 regression for landslide susceptibility mapping. *Catena* 2014; 114: 21-36.
- 579 Amir MSII, Khan MSA. An Innovative Technique of Tidal River Sediment Management to Solve the
580 Waterlogging Problem in Southwestern Bangladesh. *Coastal Management*. Elsevier, 2019, pp.
581 165-199.
- 582 Arabameri A, Rezaei K, Cerdà A, Conoscenti C, Kalantari Z. A comparison of statistical methods and
583 multi-criteria decision making to map flood hazard susceptibility in Northern Iran. *Science of*
584 *The Total Environment* 2019; 660: 443-458.
- 585 Auerbach LW, Goodbred SL, Jr., Mondal DR, Wilson CA, Ahmed KR, Roy K, et al. Flood risk of
586 natural and embanked landscapes on the Ganges-Brahmaputra tidal delta plain. *Nature Climate*
587 *Change* 2015; 5: 153-157.
- 588 Awal M. Water logging in south-western coastal region of Bangladesh: local adaptation and policy
589 options. *Science Postprint* 2014; 1: e00038.
- 590 Bai S, Lü G, Wang J, Zhou P, Ding L. GIS-based rare events logistic regression for landslide-
591 susceptibility mapping of Lianyungang, China. *Environmental Earth Sciences* 2011; 62: 139-
592 149.
- 593 Bannari A, Ghadeer A, El-Battay A, Hameed NA, Rouai M. Detection of Areas Associated with Flash
594 Floods and Erosion Caused by Rainfall Storm Using Topographic Attributes, Hydrologic
595 Indices, and GIS. Springer International Publishing, Cham, 2017, pp. 155-174.
- 596 Bonacci O, Ljubenkovic I, Roje-Bonacci T. Karst flash floods: an example from the Dinaric karst
597 (Croatia). *Nat. Hazards Earth Syst. Sci.* 2006; 6: 195-203.
- 598 Brammer H. Bangladesh's dynamic coastal regions and sea-level rise. *Climate Risk Management* 2014;
599 1: 51-62.
- 600 Brown S, Nicholls RJ. Subsidence and human influences in mega deltas: The case of the Ganges–
601 Brahmaputra–Meghna. *Science of The Total Environment* 2015; 527-528: 362-374.
- 602 Bubeck P, Botzen WJW, Kreibich H, Aerts JCJH. Detailed insights into the influence of flood-coping
603 appraisals on mitigation behaviour. *Global Environmental Change* 2013; 23: 1327-1338.
- 604 Choudhury NY, Paul A, Paul BK. Impact of costal embankment on the flash flood in Bangladesh: A
605 case study. *Applied Geography* 2004; 24: 241-258.
- 606 Croissant Y, Croissant MY. Package ‘mlogit’. 2018.
- 607 Davis J. *Statistics and Data Analysis in Geology - 3rd Edition*. John Wiley and Sons, USA, 2002.
- 608 Diaz-Nieto J, Lerner DN, Saul AJ, Blanksby J. GIS Water-Balance Approach to Support Surface Water
609 Flood-Risk Management. *Journal of Hydrologic Engineering* 2011; 17: 55-67.
- 610 Falconer R, Cobby D, Smyth P, Astle G, Dent J, Golding B. Pluvial flooding: new approaches in flood
611 warning, mapping and risk management. *Journal of Flood Risk Management* 2009; 2: 198-208.
- 612 Fox J, Weisberg S, Price B, Adler D, Bates D, Baud-Bovy G, et al. Package ‘car’. 2018.
- 613 Gain AK, Benson D, Rahman R, Datta DK, Rouillard JJ. Tidal river management in the south west
614 Ganges-Brahmaputra delta in Bangladesh: Moving towards a transdisciplinary approach?
615 *Environmental Science and Policy* 2017; 75: 111-120.
- 616 Gain AK, Schwab M. An assessment of water governance trends: the case of Bangladesh. *Water Policy*
617 2012; 14: 821-840.
- 618 Hasan MK, Kumar L, Gopalakrishnan T. Inundation modelling for Bangladeshi coasts using
619 downscaled and bias-corrected temperature. *Climate Risk Management* 2020; 27: 100207.

- 620 IPCC. Climate changes: The science of climate change, summary for policymakers and technical
 621 summary of the working group 1 report. Intergovernmental Panel on Climate Change (IPCC),
 622 Cambridge University Press, 1996.
- 623 Islam MA, Mitra D, Dewan A, Akhter SH. Coastal multi-hazard vulnerability assessment along the
 624 Ganges deltaic coast of Bangladesh: A geospatial approach. *Ocean & Coastal Management*
 625 2016; 127: 1-15.
- 626 JAXA. ALOS global digital surface model “ALOS world 3D-30m (AW3D30)”. Japan Aerospace
 627 Exploration Agency (JAXA), 2015.
- 628 Kabenge M, Elaru J, Wang H, Li F. Characterizing flood hazard risk in data-scarce areas, using a remote
 629 sensing and GIS-based flood hazard index. *Natural Hazards* 2017; 89: 1369-1387.
- 630 Khosravi K, Nohani E, Maroufinia E, Pourghasemi HR. A GIS-based flood susceptibility assessment
 631 and its mapping in Iran: a comparison between frequency ratio and weights-of-evidence
 632 bivariate statistical models with multi-criteria decision-making technique. *Natural Hazards*
 633 2016; 83: 947-987.
- 634 Kia MB, Pirasteh S, Pradhan B, Mahmud AR, Sulaiman WNA, Moradi A. An artificial neural network
 635 model for flood simulation using GIS: Johor River Basin, Malaysia. *Environmental Earth*
 636 *Sciences* 2012; 67: 251-264.
- 637 Lakhan VC. *Advances in coastal modeling*. Vol 67: Elsevier, 2003.
- 638 López-Ratón M, Rodríguez-Álvarez MX, Suarez CC, Sampedro F. OptimalCutpoints: an R package for
 639 selecting optimal cutpoints in diagnostic tests. *Journal of statistical software* 2014; 61: 1-36.
- 640 Masud MMA, Moni NN, Azadi H, Van Passel S. Sustainability impacts of tidal river management:
 641 Towards a conceptual framework. *Ecological Indicators* 2018; 85: 451-467.
- 642 McHugh ML. Interrater reliability: the kappa statistic. *Biochemia Medica* 2012; 22: 276-282.
- 643 Midi H, Sarkar SK, Rana S. Collinearity diagnostics of binary logistic regression model. *Journal of*
 644 *Interdisciplinary Mathematics* 2010; 13: 253-267.
- 645 Mojaddadi H, Pradhan B, Nampak H, Ahmad N, Ghazali AHB. Ensemble machine-learning-based
 646 geospatial approach for flood risk assessment using multi-sensor remote-sensing data and GIS.
 647 *Geomatics, Natural Hazards and Risk* 2017; 8: 1080-1102.
- 648 Mutahara M, Warner JF, Wals AE, Khan MSA, Wester P. Social learning for adaptive delta
 649 management: Tidal River Management in the Bangladesh Delta. *International Journal of Water*
 650 *Resources Development* 2018; 34: 923-943.
- 651 Nowreen S, Jalal MR, Khan MSA. Historical analysis of rationalizing South West coastal polders of
 652 Bangladesh. *Water Policy* 2014; 16: 264-279.
- 653 Planchon O, Darboux F. A fast, simple and versatile algorithm to fill the depressions of digital elevation
 654 models. *Catena* 2002; 46: 159-176.
- 655 Pradhan B. Flood susceptible mapping and risk area delineation using logistic regression, GIS and
 656 remote sensing. *Journal of Spatial Hydrology* 2010; 9.
- 657 Pradhan B, Oh HJ, Buchroithner M. Weights-of-evidence model applied to landslide susceptibility
 658 mapping in a tropical hilly area. *Geomatics, Natural Hazards and Risk* 2010; 1: 199-223.
- 659 Regmi NR, Giardino JR, Vitek JD. Modeling susceptibility to landslides using the weight of evidence
 660 approach: Western Colorado, USA. *Geomorphology* 2010; 115: 172-187.
- 661 Sabatakakis N, Koukis G, Vassiliades E, Lainas S. Landslide susceptibility zonation in Greece. *Natural*
 662 *Hazards* 2013; 65: 523-543.
- 663 Seibert J, McGlynn BL. A new triangular multiple flow direction algorithm for computing upslope areas
 664 from gridded digital elevation models. *Water Resources Research* 2007; 43.
- 665 Seijger C, Datta DK, Douven W, van Halsema G, Khan MF. Rethinking sediments, tidal rivers and
 666 delta livelihoods: Tidal river management as a strategic innovation in Bangladesh. *Water Policy*
 667 2019; 21: 108-126.
- 668 Singh RK, Hari Prasad V, Bhatt CM. Remote sensing and GIS approach for assessment of the water
 669 balance of a watershed. *Hydrological Sciences Journal* 2004; 49: 131-142.
- 670 Talchabhadel R, Nakagawa H, Kawaike K. Sediment management in tidal river: A case study of East
 671 Beel Khuksia, Bangladesh. *E3S Web of Conferences*. 40, 2018.
- 672 Talchabhadel R, Nakagawa H, Kawaike K, Hashimoto M, Sahboun N. Experimental investigation on
 673 opening size of tidal basin management: a case study in southwestern Bangladesh. *Journal of*
 674 *Japanese Society of Civil Engineers, Ser B1 (Hydraulic Engineering)* 2017; 73: I_781-I_786.

- 675 Tehrany MS, Jones S, Shabani F. Identifying the essential flood conditioning factors for flood prone
676 area mapping using machine learning techniques. *CATENA* 2019a; 175: 174-192.
- 677 Tehrany MS, Kumar L, Neamah Jebur M, Shabani F. Evaluating the application of the statistical index
678 method in flood susceptibility mapping and its comparison with frequency ratio and logistic
679 regression methods. *Geomatics, Natural Hazards and Risk* 2019b; 10: 79-101.
- 680 Tehrany MS, Lee MJ, Pradhan B, Jebur MN, Lee S. Flood susceptibility mapping using integrated
681 bivariate and multivariate statistical models. *Environmental Earth Sciences* 2014a; 72: 4001-
682 4015.
- 683 Tehrany MS, Pradhan B, Jebur MN. Flood susceptibility mapping using a novel ensemble weights-of-
684 evidence and support vector machine models in GIS. *Journal of Hydrology* 2014b; 512: 332-
685 343.
- 686 Tehrany MS, Shabani F, Neamah Jebur M, Hong H, Chen W, Xie X. GIS-based spatial prediction of
687 flood prone areas using standalone frequency ratio, logistic regression, weight of evidence and
688 their ensemble techniques. *Geomatics, Natural Hazards and Risk* 2017; 8: 1538-1561.
- 689 Thornthwaite CW, Mather JR. Instructions and tables for computing potential evapotranspiration and
690 the water balance. Drexel Institute of Technology, Centerton, NJ (EUA). Laboratory of
691 Climatology, 1957.
- 692 Van Staveren MF, Warner JF, Khan MSA. Bringing in the tides. From closing down to opening up delta
693 polders via Tidal River Management in the southwest delta of Bangladesh. *Water Policy* 2017;
694 19: 147-164.
- 695 Warner JF, van Staveren MF, van Tatenhove J. Cutting dikes, cutting ties? Reintroducing flood
696 dynamics in coastal polders in Bangladesh and the netherlands. *International Journal of Disaster
697 Risk Reduction* 2018; 32: 106-112.
- 698 WARPO. National Water Resources Database(NWRD). Water Resources Planning Organization
699 (WARPO), Bangladesh, 2018.
- 700 Wilson C, Goodbred S, Small C, Gilligan J, Sams S, Mallick B, et al. Widespread infilling of tidal
701 channels and navigable waterways in the human-modified tidal deltaplain of southwest
702 Bangladesh. *Elementa-Science of the Anthropocene* 2017; 5.
- 703 WorldPop. Bangladesh 100m Population, Version 2. University of Southampton. DOI:
704 10.5258/SOTON/WP00533 2017.
- 705 Zevenbergen LW, Thorne CR. Quantitative analysis of land surface topography. *Earth surface processes
706 and landforms* 1987; 12: 47-56.

707

The potential of Tidal River Management for flood alleviation in South Western Bangladesh

Mohammed Sarfaraz Gani Adnan^{a,c*}, Rocky Talchabhadel^b, Hajime Nakagawa^b, Jim W. Hall^a

^aEnvironmental Change Institute, School of Geography and the Environment, University of Oxford, South Parks Road, OX13QY Oxford, United Kingdom

^bDisaster Prevention Research Institute, Kyoto University, Japan

^cDepartment of Urban and Regional Planning, Chittagong University of Engineering and Technology (CUET), Chittagong 4349, Bangladesh

Supplementary tables

Table S1| Major dataset used in this research

Data	Description	Sources
Digital elevation model (DEM)	The Advanced Land Observing Satellite (ALOS) DEM of 30m spatial resolution	(JAXA, 2015)
Land use	Land use and land cover data for 2013	(http://www.espadelta.net/) (Mukhopadhyay et al., 2018)
Population	Gridded population data of 90m spatial resolution	(WorldPop, 2017)
Precipitation data	Gridded (5km grid points) precipitation data of 10-day temporal resolution from 1965-2012	Bangladesh Meteorological Department (www.bmd.gov.bd/)
Soil texture data	Topsoil texture data with attributes of texture types, such as ‘silt loam’, ‘clay’, ‘silty clay’, etc.	Bangladesh Agricultural Research Council (http://www.barc.gov.bd/)
Soil permeability	Soil permeability level (‘very low’ to ‘very high’)	Bangladesh Agricultural Research Council (http://www.barc.gov.bd/)
Spatial data	Geographic Information System (GIS) data on polder boundary, polder number, river lines etc.	The Water Resources Planning Organization (WARPO) (www.warpo.gov.bd/)

Table S2| Flood observation data used to develop and validate the flood susceptibility model

Dataset	Flood points	Non-flood points	Total
Training dataset	426	274	700
Test dataset	160	140	300
Total	586	414	1000

Table S3| Multicollinearity diagnosis of selected flood conditioning factors

Selected variables	Variance inflation factor (VIF)	Mean VIF
Aspect	1.049	
Elevation	2.445	
Slope	1.274	
Curvature	1.469	
Land subsidence	1.179	
Precipitation	1.544	
SPI	1.734	1.397
Land use	1.392	
Soil texture	1.204	
Soil permeability	1.315	
Distance from drainage channels	1.058	
Distance from rivers	1.098	

Table S4| Population and land uses in flood susceptible areas of varying degrees

Exposure	Categories of flood probability				
	0 – 0.2	0.2 – 0.4	0.4 – 0.6	0.6 – 0.8	0.8 – 1
Population (%)	38	9	8.5	13.5	31
Land use (% of area)					
Shrimp culture	9.4	5.0	6.5	16.8	62.2
Rice field	21.5	6.5	7.0	13.8	51.2
Mixed rice field, shrimp, and other fish culture	0.7	1.8	2.9	4.4	90.2
Mangrove	34.7	9.7	18.7	21.5	15.3
Shrimp and other fish culture	2.0	3.7	3.9	4.1	86.2
Other crop agriculture land	25.6	8.0	8.0	18.1	40.3
Freshwater fish culture	13.5	5.7	6.2	10.8	63.9
Settlement with Homestead	48.0	10.4	9.8	14.6	17.3
Vegetation (Rural)					
Settlement with Homestead	71.4	8.1	6.8	6.7	7.0
Vegetation (Urban)					
Others	0.2	0.2	0.5	11.7	87.4

Supplementary figures

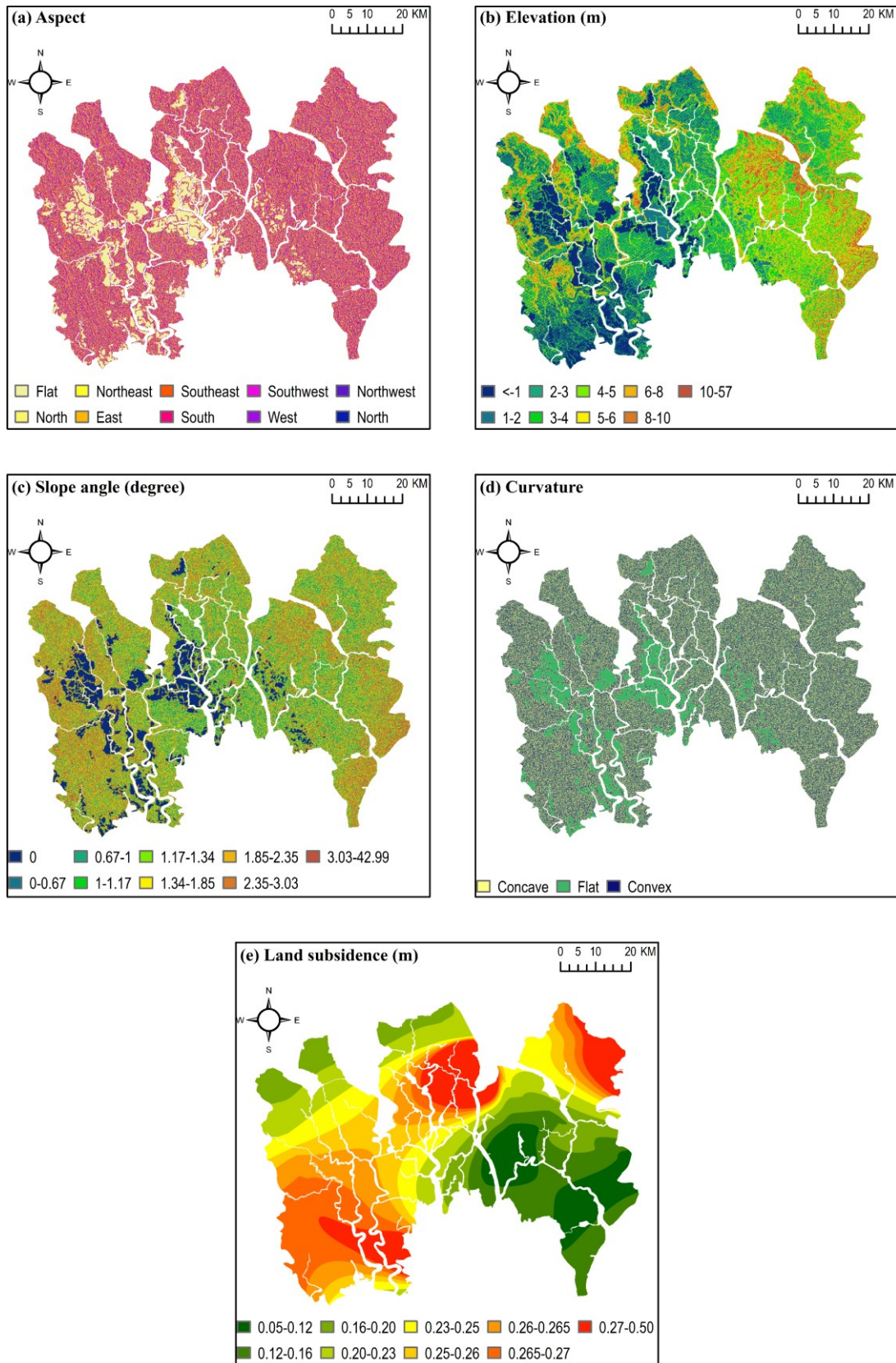


Fig. S1. Topographic factors contribute to flood

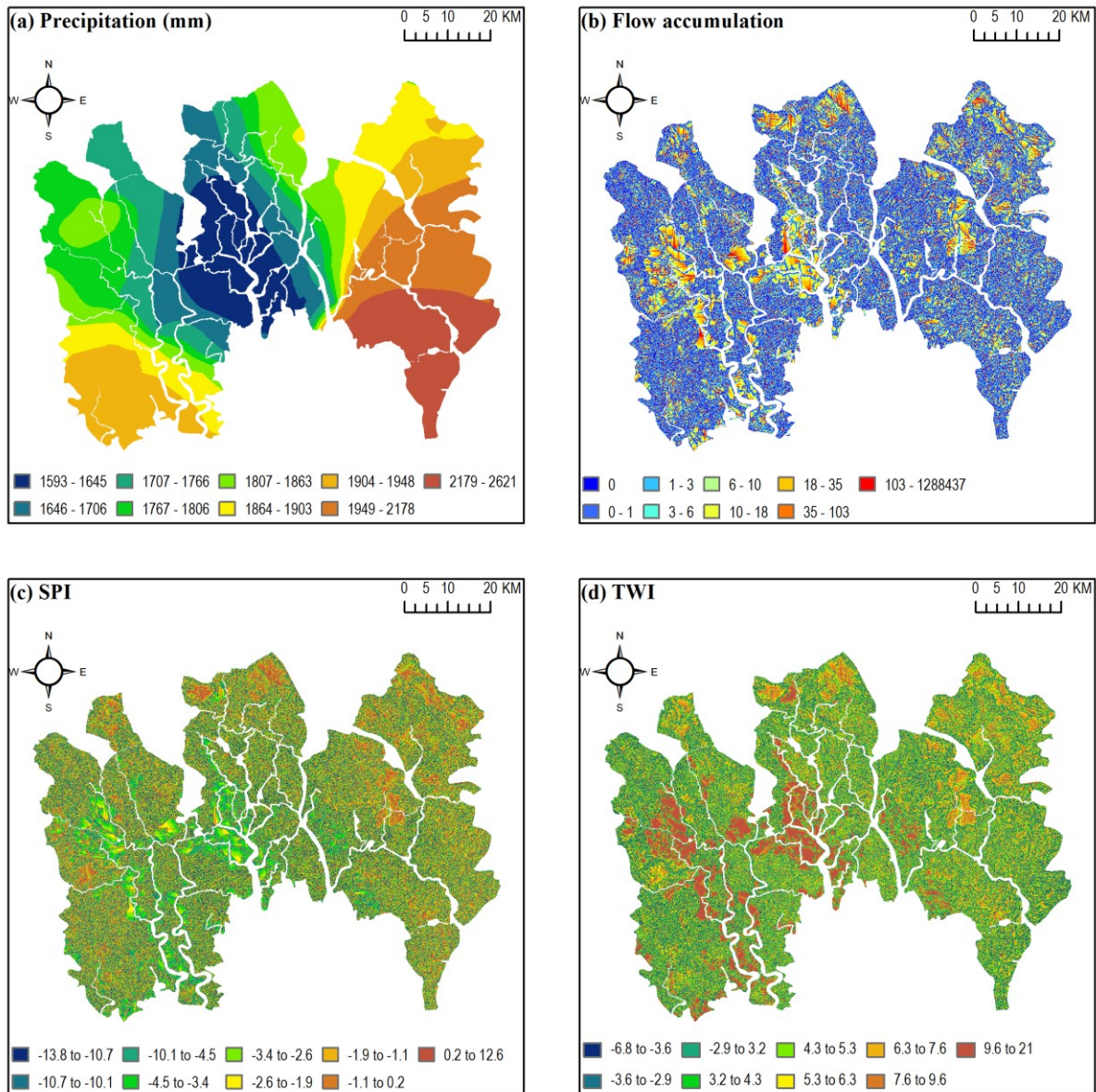


Fig. S2. Hydrological factors influence flood

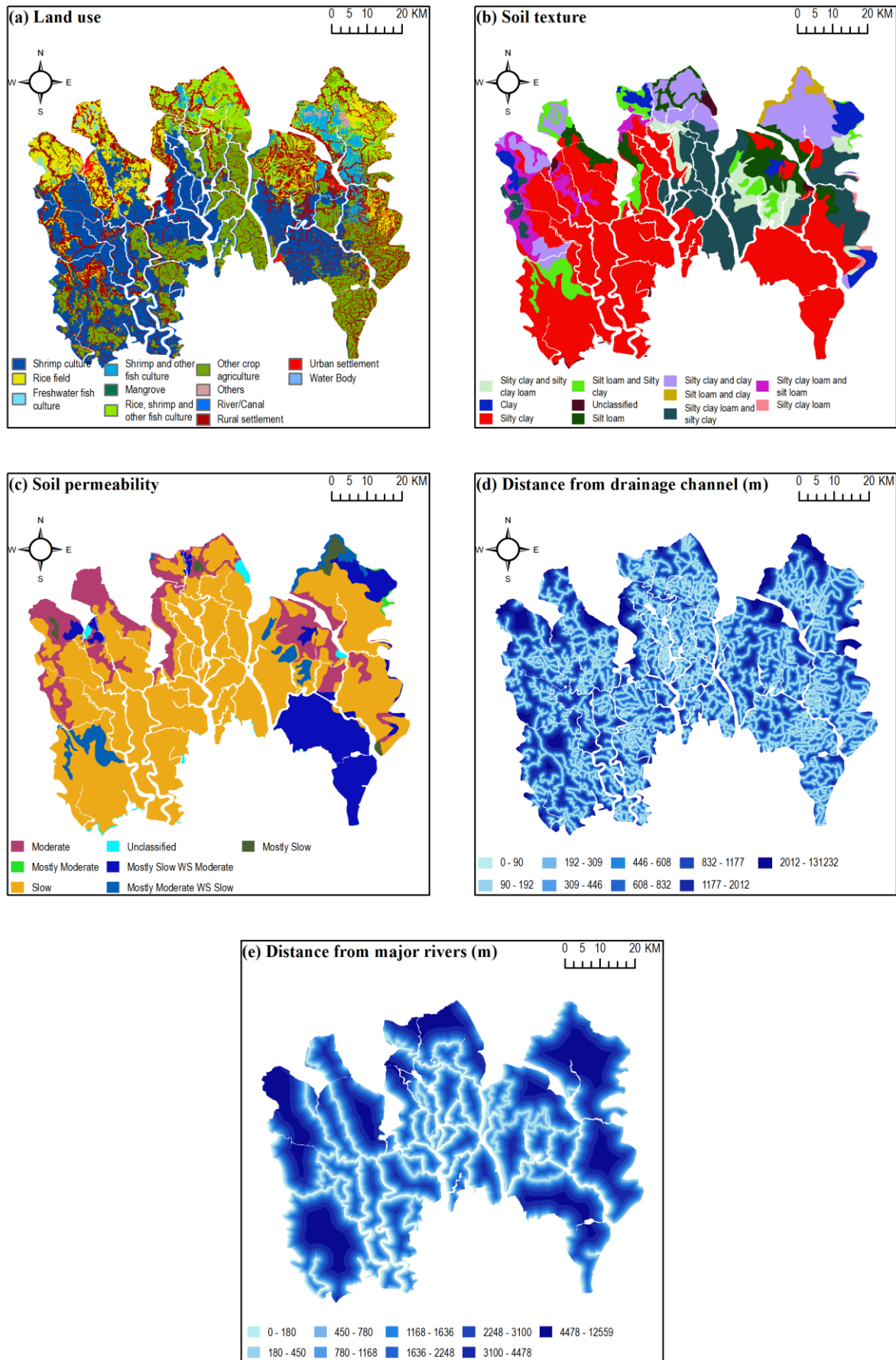


Fig. S3. Anthropogenic, geological, and locational factors influencing flood

Experimental study for sediment transport modelling

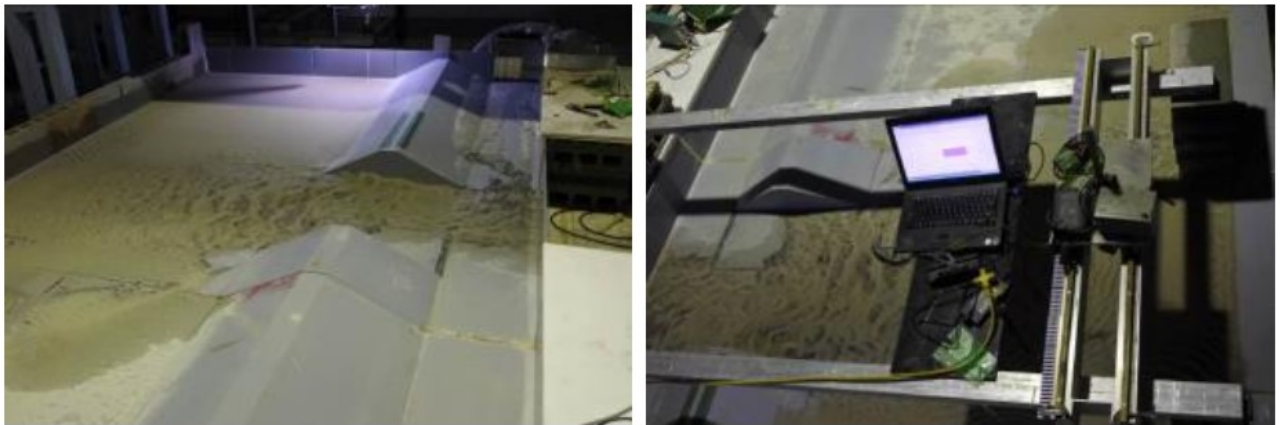


Fig. S4. Experimental facility: photos of bed level (left) and bed level measurement using laser displacement sensor (right) case II

Source:(Talchabhadel et al., 2017a)

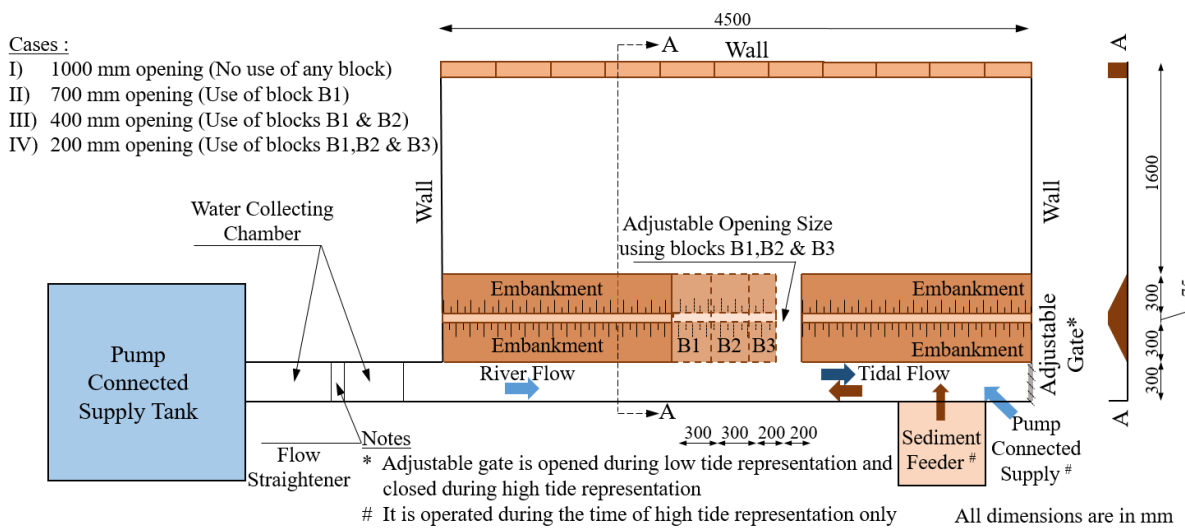


Fig. S5. Schematic view of the experimental setup

Source: (Talchabhadel et al., 2016; Talchabhadel et al., 2018)

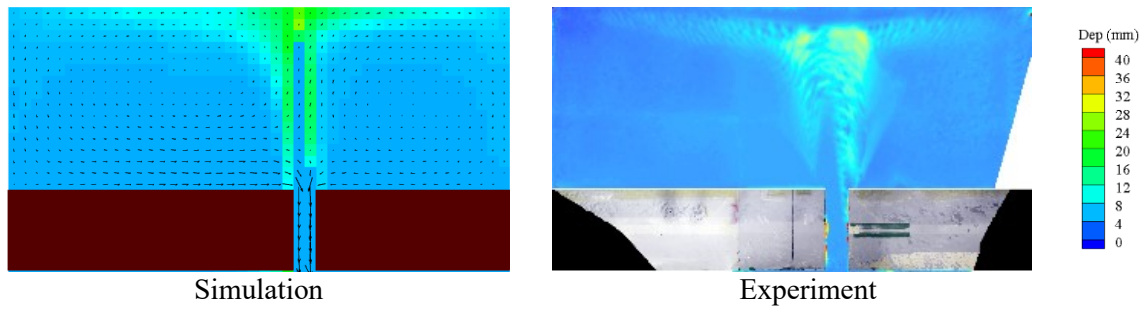


Fig. S6. Sample comparison of simulated and experimental results of deposited sediment after repetitive tidal movement

Source:(Talchabhadel et al., 2017a; Talchabhadel et al., 2017b)

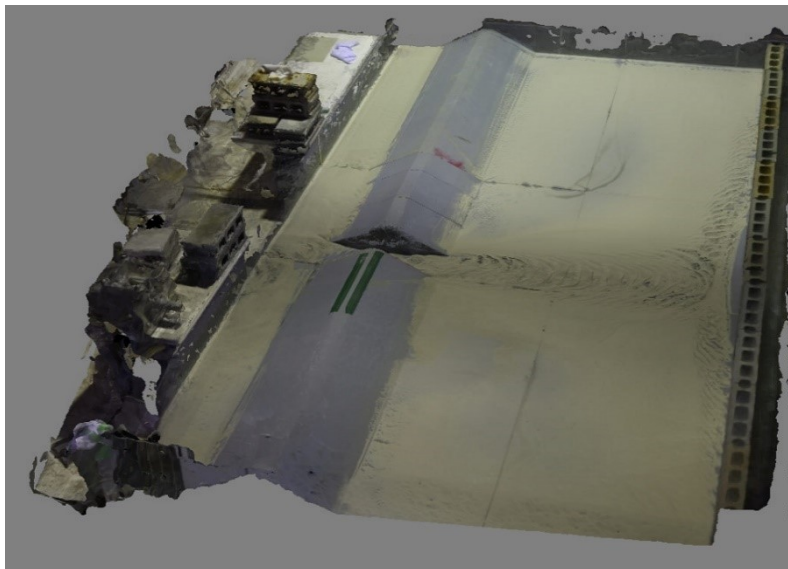


Fig. S7. Perspective view (3D spatial data from digital images)

Source: (Talchabhadel et al., 2017b)

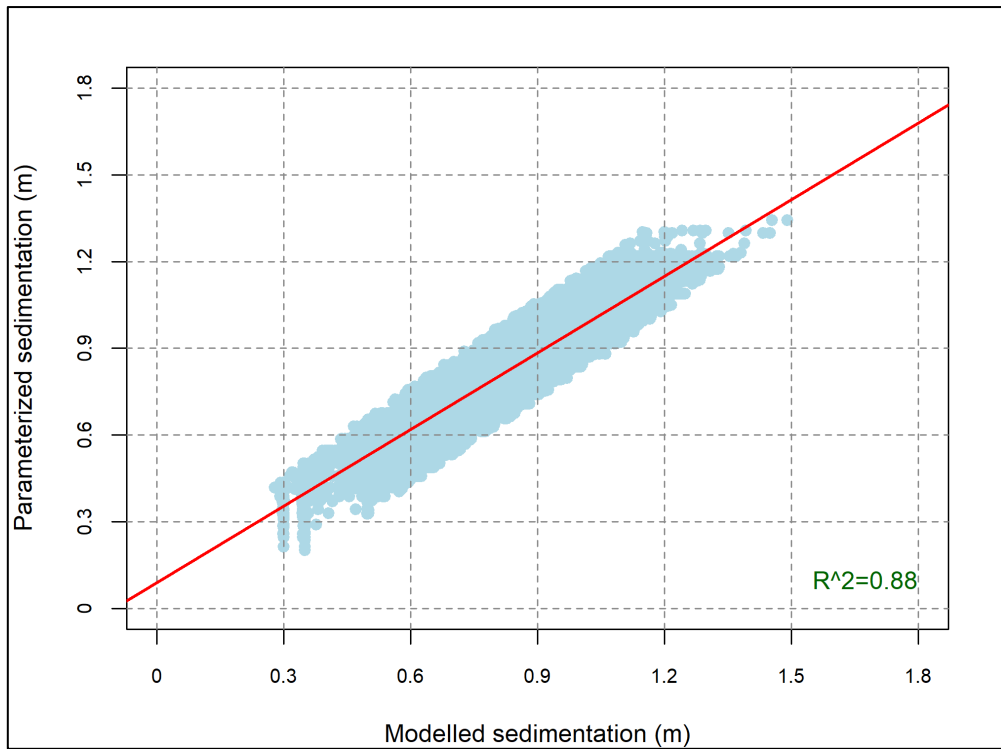


Fig. S8. Validation of suitability model to select candidate TRM sites

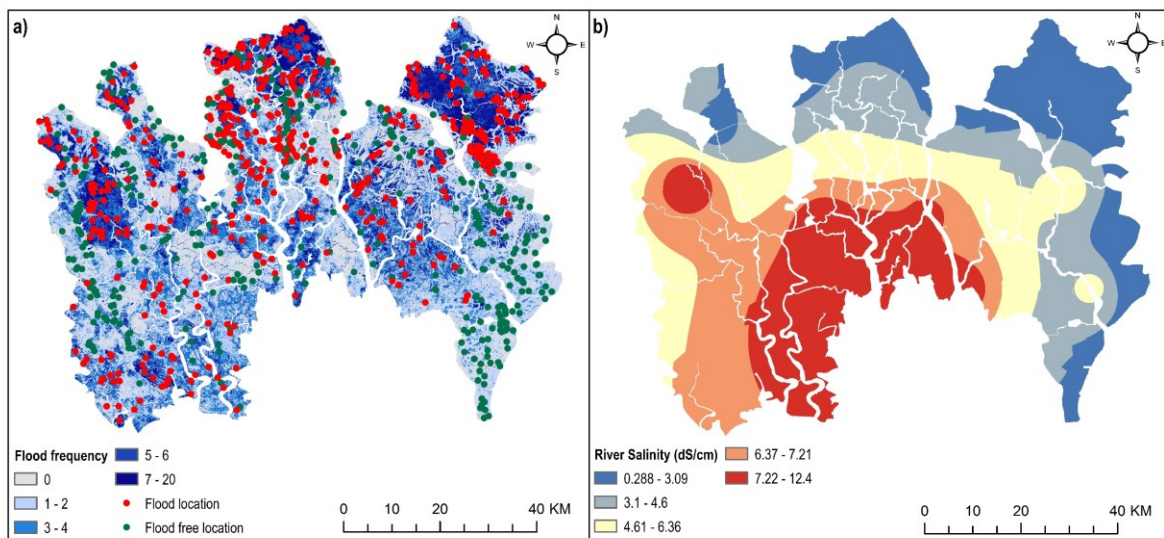


Fig. S9. a) Flood inventory map; b) River salinity map

References

- JAXA. ALOS global digital surface model “ALOS world 3D-30m (AW3D30)”. Japan Aerospace Exploration Agency (JAXA), 2015.
- Mukhopadhyay A, Hornby DD, Hutton CW, Lázár AN, Amoako Johnson F, Ghosh T. Land Cover and Land Use Analysis in Coastal Bangladesh. In: Nicholls RJ, Hutton CW, Adger WN, Hanson SE, Rahman MM, Salehin M, editors. *Ecosystem Services for Well-Being in Deltas: Integrated Assessment for Policy Analysis*. Springer International Publishing, Cham, 2018, pp. 367-381.
- Talchabhadel R, Nakagawa H, Kawaike K. Experimental study on suspended sediment transport to represent Tidal Basin Management. *Journal of Japanese Society of Civil Engineers, Ser B1 (Hydraulic Engineering)* 2016; 72: I_847-I_852.
- Talchabhadel R, Nakagawa H, Kawaike K, Hashimoto M, Sahboun N. Experimental investigation on opening size of tidal basin management: a case study in southwestern Bangladesh. *Journal of Japanese Society of Civil Engineers, Ser B1 (Hydraulic Engineering)* 2017a; 73: I_781-I_786.
- Talchabhadel R, Nakagawa H, Kawaike K, Ota K. Experimental and Numerical Study of Tidal Basin Management around Link Canal: A Case Study of Bangladesh. *DPRI Annuals* 2017b.
- Talchabhadel R, Ota K, Nakagawa H, Kawaike K. Three-Dimensional Simulation of Flow and Sediment Transport Processes in Tidal Basin. *Journal of Japan Society of Civil Engineers* 2018; 74: I_955-I_960.
- WorldPop. Bangladesh 100m Population, Version 2. University of Southampton. DOI: 10.5258/SOTON/WP00533 2017.